# Airborne investigation of the aerosols–cloud interactions in the vicinity and within a marine stratocumulus over the North Sea during EUCAARI (2008)

Suzanne Crumeyrolle, Ralf Weigel, Karine Sellegri, Greg Roberts, Laurent Gomes, Andreas Stohl, Paolo Laj, Géraud Momboisse, Thierry Bourrianne, Vincent Puygrenier, et al.

# Airborne investigation of the aerosols–cloud interactions in the vicinity and within a marine stratocumulus over the North Sea during EUCAARI (2008)

S. Crumeyrolle [a, b, *], R. Weigel [a, c], K. Sellegri [a], G. Roberts [d], L. Gomes [d], A. Stohl [e], P. Laj [a, g], G. Momboisse [d], T. Bourianne [d], V. Puygrenier [d, f], F. Burnet [d], F. Chosson [h], J.L. Brenguier [d], J.M. Etcheberry [d], P. Villani [a], J.M. Pichon [a], A. Schwarzenboeck [a]

[a] *Laboratoire de Météorologie Physique, CNRS, Université Blaise Pascal, UMR6016, Aubière cedex, France*
[b] *NASA Langley Research Center, Hampton, VA 23666, USA*
[c] *Institute for Physics of the Atmosphere, Johannes Gutenberg University, Mainz, Germany*
[d] *Centre National de Recherches Météorologiques, URA 1357, Météo-France, Toulouse, France*
[e] *Norwegian Institute for Air Research, Kjeller, Norway*
[f] *Laboratoire des Science du Climat et de l'Environnement, CNRS, France*
[g] *Departement of Atmospheric and Oceanic Sciences, McGill University, Montreal, Canada*
[h] *Laboratoire de Glaciologie et Géophysique de l'Environnement, UMR 5183, Université de Grenoble 1/CNRS, Grenoble, France*

## HIGHLIGHTS

- Observations of aerosol properties within and in the vicinity of a stratocumulus.
- Decrease of the aerosol concentration in the 200 m above the cloud due to entrainment.
- 'Hoppel minimum' observed below the cloud layer.
- New particle formation observed above the cloud layer.
- Strong increase of nitrate aerosol within the cloud.

## ARTICLE INFO

*Article history:*
Received 18 December 2012
Received in revised form
17 August 2013
Accepted 20 August 2013

*Keywords:*
Aerosols
CCN
In-situ measurements
Stratocumulus
Activation

## ABSTRACT

Within the European Aerosol Cloud Climate and Air Quality Interactions (EUCAARI) project, the Meteo France research aircraft ATR-42 was operated from Rotterdam (Netherlands) airport during May 2008, to perform scientific flights dedicated to the investigation of aerosol–cloud interactions. The objective of this study is to illustrate the impact of cloud processing on the aerosol particle physical and chemical properties. The presented results are retrieved from measurements during flight operation with two consecutive flights, first from Rotterdam to Newcastle (United Kingdom) and subsequently reverse along the same waypoints back to Rotterdam using data measured with compact Time of Flight Aerosol Mass Spectrometer (cToF-AMS) and Scanning Mobility Particle Sizer (SMPS). Cloud-related measurements during these flights were performed over the North Sea within as well as in close vicinity of a marine stratocumulus cloud layer. Particle physical and chemical properties observed in the close vicinity, below and above the stratocumulus cloud, show strong differences: (1) the averaged aerosol size distributions, observed above and below the cloud layer, are of bimodal character with pronounced minima between Aitken and accumulation mode, very likely due to cloud processing. (2) the chemical composition of aerosol particles is strongly dependent on the position relative to the cloud layer (vicinity or below/above cloud). In general, the nitrate and organic relative mass fractions decrease with decreasing distance to the cloud, in the transit from cloud–free conditions towards the cloud boundaries. This relative mass fraction decrease ranges from a factor of three to ten, thus leading to an increase of the sulfate and ammonium relative mass concentrations while approaching the cloud layer. (3), the chemical composition of cloud droplet residuals, analyzed downstream of a Counterflow virtual Impactor (CVI) inlet

* Corresponding author. NASA Langley Research Center, 21 Langley Blvd, MS 483, Bldg 1250, Room 125, Hampton, VA 23681, USA. Tel.: +1 757 392 6856; fax: +1 757 864 4344.
*E-mail address:* suzanne.crumeyrolle@gmail.com (S. Crumeyrolle).

indicates increased fractions of mainly soluble chemical compounds such as nitrate and organics, compared to non cloud processed particles. Finally, a net overbalance of nitrate aerosol has been revealed by comparing cloud droplet residual and non cloud processed aerosol chemical compositions. Conclusively, this study highlights gaps concerning the sampling strategy that need to be addressed for the future missions.

## 1. Introduction

Aerosols originate either from natural sources (e.g. mineral dust, sea salt, ash, biogenic aerosol or ablation material of meteorites) or from emissions by anthropogenic activities (e.g. soot, smoke, and other traffic or industrial emissions, e.g. lead or mercury particles (Murphy et al., 1998)). Those aerosol particles which undergo long range transport may have a particularly strong influence on the climate directly by absorbing and reflecting shortwave solar radiation (Haywood et al., 2003; Intergovernmental Panel on Climate Change, 2007) and indirectly by modification of cloud structure as well as their microphysical properties (Lohmann et al., 2004).

Aerosol–cloud interactions depend on aerosol particle properties such as number concentration, size, chemical composition, hygroscopic properties and mixing state (Roberts et al., 2001; Sellegri et al., 2003; Cubison et al., 2008; Wang et al., 2011). In addition, the interaction of aerosols with steam or cloud water depends on the type of involved clouds, including continental or maritime, convective or stratiform, and liquid or ice phase clouds (Reutter et al., 2009; Andrejczuk et al., 2010). Atmospheric aerosol particles affect cloud formation by acting as cloud concensation nuclei (CCN) and ice nuclei (IN) (Harrison, 2000). In return, aerosol properties are modified by in-cloud processes (Hoppel et al., 1994; Levin et al., 1996). Gaseous compounds and aerosol particles are ingested by cloud droplets through absorption/condensation and activation, respectively (Flossmann et al., 1985; Pruppacher and Klett, 1997) and, thus, may dissolve, dissociate, and undergo chemical reactions (Seinfeld and Pandis, 1998). For example, aqueous-phase chemistry in cloud droplets significantly contributes to sulfate and nitrate aerosol production in the atmosphere (Hegg, 1985; Walcek and Taylor, 1986; Hayden et al., 2008). Previous studies estimate that globally up to 80% of the sulfate total production is through aqueous-phase oxidation (Barth et al., 2000). Clouds also act as an efficient sink for aerosols and other soluble tracers (e.g. $NH_3$, $SO_2$, $CO_2$ etc.) through scavenging by precipitation. However, a large portion of the cloud-processed particulate matter, often physically and chemically altered, will be released back to the atmosphere upon cloud dissipation and evaporation as a large faction of clouds globally are non-precipitating (Seigneur and Saxena, 1988; Karamchandani and Venkatram, 1992). The released particles are then chemically modified due to a coating of soluble compounds (Hoppel et al., 1994; Wurzler et al., 2000) causing modified their hygroscopic properties (Levin et al., 1996; Crumeyrolle et al., 2008) and increasing mean diameter of these particles. Rain is an effective mechanism for aerosol removal from the atmosphere and is caused by two processes: (a) if below-clouds a particle in the BL, is collected by a falling raindrop ("below-cloud scavenging", BCS); (b) if a particle in a cloud or at cloud base, where supersaturated conditions exist, becomes a cloud droplet by the nucleation scavenging process (Komppula et al., 2005). In-cloud interstitial aerosol may also be scavenged by coagulation with cloud droplets and collection by falling raindrops.

Nevertheless, experimental evidences by in-situ investigations of in-cloud aerosol processing are rare and often limited to ground-based studies on orographic clouds (Bower et al., 1997). Hill-top clouds are specific clouds that form when supersaturation is driven by orography and which are often very large compared to other type of clouds, in particular marine stratocumulus clouds. Marine boundary layer clouds cover a large fraction of the planetary ocean ($\sim$30% according to Warren et al., 1988) and their albedo is about 10 times larger than the one of the underlying dark ocean surface. This means that marine boundary layer clouds may crucially influence the Earth's radiation budget (Hartmann et al., 1992).

The study presented here has been conducted within the European Aerosol Cloud Climate and Air Quality Interactions (EUCAARI, Kulmala et al., 2009, 2011) project. The EUCAARI project has been initialized to investigate the effects of aerosol particles on climate and air quality. Quantifying the effect of aerosols on the planet's radiative balance is one of the most urgent tasks in currently made efforts to understand future climate change (IPCC, 2007). As a whole, the contribution of the various aerosol sources, the role of long-range transport, and the contribution of primary and secondary particulate matter to the atmospheric aerosol concentrations over Europe are still not well known. Particularly uncertain remain the aerosol parameters influencing the radiative balance and the properties of clouds (Adams and Seinfeld, 2002; Kaufman et al., 2002; Spichtinger and Cziczo, 2008). The EUCAARI observational system consists of long-term and spatially extensive surface-based measurements, including the European network of supersites for aerosol research (EUSAAR, Philippin et al., 2009).

Within the framework of the EUCAARI project an intensive measurement campaign including the deployment of European instrumented research aircraft (DLR Falcon-20, FAAM BAe-146, NERC Dornier Do-128, Météo-France ATR-42 and French Falcon-20) has been performed in May 2008. Some of the results from these flights have already been reported for example by Mirme et al. (2010), Crumeyrolle et al. (2010). The study presented here focuses on the impact of a marine stratocumulus on aerosol physical and chemical properties based on airborne measurements. The airborne sampling strategy and the onboard instrumentation are described in Section 2. Size distributions, mass concentrations and chemical composition of aerosol particles observed near the cloud and inside the cloud are presented in the Section 3.

## 2. Instrumentation

Within the EUCAARI project, the intensive measurement campaign dedicated to aerosol and cloud studies was carried out between the 1st and 31st of May 2008 in the Netherlands including both airborne and ground measurements. The ATR-42 research aircraft, operated by SAFIRE (Service des Avions Français Instrumenté pour la Recherche en Environnement), was based at the Rotterdam airport and was equipped with comprehensive scientific instrumentation to perform aerosol–cloud studies (Crumeyrolle et al., 2008; Matsuki et al., 2010). A total of 22 research flights were performed between 2 May and 30 May 2008 (Crumeyrolle et al., 2010).

The ATR-42 was equipped with the Community Aerosol Inlet (CAI) for aerosol measurements in cloud-free conditions and a Counterflow Virtual Impactor (CVI, Ogren et al., 1985; Schwarzenboeck et al., 2000) that was used during in-cloud measurements. The isokinetic CAI is

based on the University of Hawaï shrouded solid diffuser inlet designed by A. Clarke (personal communication) and modified by Meteo France. The CAI inlet allows for sampling submicron and partly supermicron particles with an upper 50% sampling efficiency for particle sizes at $D \sim 5$ μm (McNaughton et al., 2007). Thus, switching between the CVI during in-cloud conditions and the CAI in cloud-free conditions allowed for direct sampling of either the cloud residual or cloud free total aerosol particles.

The CVI is designed to exclusively collect cloud elements (cloud droplets and ice crystals; $D > 5$ μm of aerodynamic particle diameter), while essentially rejecting interstitial aerosol particles. Because droplets or crystals in a large sampling volume are impacted into a relatively small sample stream, their number concentrations and water contents within the CVI are significantly enhanced over their ambient values. This enhancement factor is equal to the ratio of the air sample flow rate impinging on the probe tip to the sample flow rate within the inlet probe (Twohy et al., 2003). The averaged enhancement factor used to correct the EUCAARI data was about 3.7. As shown in Sellegri et al. (2003), the efficiency coefficient concerning aerosol aspiration, transmission and transport through the inlet was obtained by comparing in cloud aerosol number concentrations, cloud-free particle concentrations, and whole air aerosol concentrations. During our study, aerosol number densities were not measured simultaneously under various cloud conditions. Thus, we use the liquid water content (LWC) measurements outside and inside the CVI, respectively, to evaluate both the adequacy of the lower size cut of the CVI to sample cloud droplets and the sampling losses. The comparison between the LWC measured by the Gerber probe in and outside the CVI show a strong correlation. Indeed, the CVI measurements are overestimating the LWC by a factor of 0.1 which is in the range of the uncertainty in both measurements. According to this results, the mass concentration measured downstream the CVI are considered as being representative for the cloud residuals mass concentrations.

Two Scanning Mobility Particle Sizers (SMPS) measured size distributions between 20 and 500 nm in diameter of particles entering the CAI probe: one SMPS was operated at ambient conditions and the second SMPS measured downstream of a denuder that heats the aerosol up to 280 °C. The SMPS systems consisted of a Krypton aerosol neutralizer (Kr-85), a DMA (Differential Mobility Analyzer) as described by Villani et al. (2007) and a TSI model 3010 condensation particle counter (CPC). Typically, the time span for the SMPS to scan over the detectable particle diameter range from 20 to 500 nm was set to 90 s. SMPS submicron aerosol size distributions were processed, taking into account the particles electrical charging probabilities, the CPC counting efficiencies and the DMA transfer functions.

An Aerodyne compact Time of Flight Aerosol Mass Spectrometer (cToF-AMS, Drewnick et al. (2005); Canagaratna et al. (2007)) was applied for the EUCAARI mission to analyze in quasi-real time the chemical composition of the non-refractory aerosol particles collected by the CAI and CVI probes. The notation non-refractory includes all aerosol compounds that evaporate in a few milliseconds at a temperature of ~600 °C on a vaporizer surface in the high vacuum section of the cToF-AMS, prior to the mass spectrometric analysis. In practice, cToF-AMS measurements exclude the detection of black carbon, crustal materials, and sea salt/sodium chloride. Even though, a fraction of non-refractory species internally mixed with refractory species (e.g., organics internally mixed with black carbon) can be quantitatively detected with the AMS (Katrib et al., 2005; Slowik et al., 2004). The non-refractory particle species that are vaporized are then subjected to electron impact (EI) ionization, which forms positive ions that are analyzed using a Time-of-Flight mass spectrometer. For typical accumulation mode particles, the sampling efficiency (predominantly limited by the aerodynamic lens, Zhang et al., 2004) is close to 100% and the AMS quantitatively measures mass loadings (Liu et al., 2007). Laboratory measurements showed that particle diameters ($D$) larger than 800 nm are excluded from analysis with our cToF-AMS, whereas particles with 600 nm in diameter are assumed to be detected with efficiency close to 100%.

The AMS-measured mass concentrations of non-refractory aerosol compounds need to be corrected in order to consider a variable efficiency of an AMS to collect aerosol particles. The collection efficiency (CE) of an AMS is the fraction of given ambient particles that are able to transmit through the instrument and to reach the AMS detector for being analyzed. The general components influencing the CE were described by Huffman et al. (2005). During laboratory and field studies several solutions were established to correct the measured mass concentration for the CE of an AMS. Some of these are described and evaluated in a recent publication by Middlebrook et al. (2012). Based on field measurements, Crosier et al. (2007) provided a CE correction based on the aerosol chemical composition, i.e. the quantitative ratio of nitrate and sulfate compound in the aerosol particles; Matthew et al. (2008) furthermore suggest from laboratory studies that the CE is in particular a matter of the particles phase (liquid/solid) – this concludes that the relative humidity (RH) in the aerosol line upstream of the AMS entrance significantly influences the CE (Middlebrook et al., 2012).

During the EUCAARI aircraft operation of the cToF-AMS, unfortunately, no device for either measuring or controlling the aerosol line RH was implemented between the aerosol inlet and the AMS entrance. As the sampled air is heated due to deceleration of the air stream inside the inlet (CVI or CAI), and as the air flow inside the aircraft cabin is further heated as the cabin temperature exceeded ambient air temperature outside the aircraft by at least 15 °C, it is conceivable that the RH in the aerosol line is significantly decreased. The cToF-AMS used during EUCAARI/IMPACT was additionally equipped with a Pressure Controlled Inlet (PCI), similarly to the system described by Bahreini et al. (2008). The PCI further aids the decrease of the air flows RH. Thus, on can assume that aerosol particles collected through the CVI and the CAI are significantly dried before reaching the AMS entrance, as a rough estimate to RH < 30%. Without knowing the exact RH values in the aerosol line, a correction for the CE was done according to the-mostly accepted correction procedure (at the time of the EUCAARI data processing) as described by Crosier et al. (2007). Middlebrook et al. (2012) show that only in a certain intermediate range of aerosols ammonium nitrate mass fraction the Crosier et al. (2007) CE correction may lead to an overestimation of measured mass concentration of 15–20% in maximum. Over the largest range of the ammonium nitrate mass fraction, as indicated by Middlebrook et al. (2012), the herein used CE correction generally holds comparably well and, thus, is assumed to do so also for the EUCAARI cToF-AMS data set.

Generally, cToF-AMS measurements deliver size segregated aerosol chemical composition analyses with alternating operation modes, the Particle Time of Flight (PToF) and the Mass Spectrometer (MS) mode. Due to a not identified instrumental malfunction in the particle sizing PToF mode of our cToF-AMS this study focuses on the measurement in the MS mode (10 s sampling time, 23 s temporal resolution) delivering exclusively the non-refractory aerosol chemical composition over the entire AMS measurement size range.

Thus, the aerosol size distribution (SMPS), as well as the non-refractory aerosol chemical composition (cToF-AMS), is measured simultaneously during cloud-free periods while only aerosol chemical composition is measured during 'in-cloud' periods. This

**Table 1**
Acronyms list.

| BL | Boundary layer |
|---|---|
| C | Above/Under cloud segment |
| CAI | Community Aerosol Inlet |
| CCN | Cloud condensation nuclei |
| CPC | Condensation Particle Counter |
| CVI | Counterflow Virtual Impactor |
| DMA | Differential Mobility Analyzer |
| D | Particle diameters |
| EAP | Efficiency of Activation and in-cloud Production |
| EUCAARI | European Aerosol Cloud Climate and Air Quality Interactions |
| FT | Free Troposphere |
| I | In cloud segment |
| m [asl] | Meters above sea level |
| RF# | Research Flight number# |
| SC | Stratocumulus |
| SMPS | Scanning Mobility Particle Sizer |
| ToF-AMS | Time of Flight Aerosol Mass Spectrometer |
| V | Vicinity of the cloud segment |

latter fact is due to the SMPS scan durations that are not adapted for use in heterogeneous cloud fields with the CVI inlet. In order to validate the data set, mass concentrations derived from the size distribution measurements (SMPS and Passive Cavity Aerosol Spectrometer Probe – PCASP-100) and AMS measured mass concentrations (assuming a particle collection efficiency –CE- of 0.5) during cloud free periods were compared and found to be in appropriate agreement. In order to make reading of this study easier, Table 1 gives an overview of the acronyms used in this study.

## 3. Experimental strategy

In this study, we selected two cloud research flights performed on 15 May 2008 over the North Sea from Rotterdam to Newcastle during the morning (06:19–09:50 UTC) and the return flight from Newcastle to Rotterdam during the afternoon (11:49–15:06 UTC). The measurements during these two research flights (RF51 and RF52) were performed in- and outside a stratocumulus cloud layer on 15 May 2008. The rather equal flight trajectories of these two flights as well as the brightness temperature from MODIS are presented in Fig. 1. The stratocumulus field that was studied is located in the northern part of the domain while cirrus is present in the southern part.

The different flight segments related to the stratocumulus (sc) cloud layer are represented in Fig. 2: green segments that correspond to cloud-free periods named vicinity to the stratocumulus (V segments), black segments that are related to measurements below/above cloud layer (C segments), whereas purple segments correspond to 'in-cloud' measurements sampling the cloud residual aerosol via the CVI inlet (I segments). For each flight segment, respective time period, segment position relative to the cloud layer, flight altitude as well as the virtual and equivalent potential temperature are listed in Table 2 (morning flight, RF51) and Table 3 (afternoon flight, RF52).

### 3.1. Structure of the atmosphere

Remote sensing observations, performed by the nadir-looking RASTA radar (Protat et al., 2004) on board the ATR-42, were used to specify the precipitating or non-precipitating character of this stratocumulus (Brenguier et al., 2011). The radar reflectivities were similar (about −20dBZ) during the morning and afternoon flights and the associated mean Doppler velocity was between −2 and −4 $m^{-1}$. The reflectivities are characteristic for drizzle regime. Drizzle drops reached lower altitudes during the morning (down to altitudes of 300 m [asl]) than during the afternoon (down to 500 m [asl]) before they evaporated. As the cloud droplets are falling below the cloud base, the evaporative cooling of these cloud droplets is dividing the boundary layer into two different layers. The lower layer is then connected to the surface while the other is connected to the cloud. To facilitate reading, a conceptual cloud scheme is presented in Fig. 3 summarizing the state of the lower troposphere for the cloud free and the precipitating stratocumulus conditions. During cloud free conditions the boundary layer appears to be a well-mixed layer while the layer below the stratocumulus is decoupled from the surface layer due to drizzle evaporation under the cloud base (Feingold et al., 1998).

Using the cloud vicinity thermodynamical measurements, the height of the boundary layer was estimated at 600 m [asl]. Fig. 4 represents the vertical profiles of the potential temperature (a), the vapor mixing ratio (a) as well as the aerosol number concentrations (b) measured onboard the ATR-42 during the cloud periods as a function of the altitude during the morning and afternoon (RF51 and RF52) flights. The top of the boundary layer, corresponding also to the stratocumulus base (600 m [asl]), is clearly marked on the vapor mixing ratio as well as on the aerosol number concentration profiles. Moreover in this layer (BL), the vertical profiles performed during the afternoon flight (RF52) highlight the presence of two distinct layers. In the lower layer (<450 m [asl]), the aerosol number concentrations reach 1000 $cm^{-3}$ and the water vapor mixing ratio is larger than 6.2 g $kg^{-1}$. In the upper layer (in between 450 and 600 m [asl]), right below the cloud, the aerosol number concentrations are in average 500 $cm^{-3}$ while the water vapor mixing ratios are lower than 5.9 g $kg^{-1}$. The BL decoupling level corresponds to the lower altitude reached by the drizzle drops during the afternoon. The measurements performed within the surface layer during the afternoon flight are thus not comparable with the morning flight measurements at the same altitude.

Within an altitude range of 200 m above the stratocumulus, these thermodynamic parameters show also a considerable variability due to the mixing of moist and cold air from the cloud layer with dry and warmer air originating from the free troposphere. Therefore, the measurements immediately above the cloud layer are not representative for the free troposphere but rather for the inversion layer above cloud top – allegorizing a transition region which is influenced by cloud related processes.

### 3.2. Air masses transport

In order to determine the transport pathways of the sampled air masses we used the FLEXPART model (Stohl et al., 1998, 2005). The FLEXPART model has been run for both EUCCARI flights to calculate the 3 days back trajectories using the exact location of the ATR-42 as the final point of the air mass trajectory. During the 15th May 2008, the same air mass pathway was depicted by Flexpart for all ATR-42 locations within both layers. Indeed, the model revealed that air masses coming from the North–East were sampled with the ATR-42 during the morning (RF51) and also the afternoon flight (RF52, Fig. 5). Furthermore, the wind direction and wind speed observed on board the ATR-42 within specific flight segments, in the boundary layer and in the free troposphere, are illustrated in Fig. 6. The prevailing wind approached the air sectors of measurements from North-East directions for both flights and both layers, as derived from FLEXPART calculated air mass pathways. The FLEXPART results as well as the in-situ measurements are showing the very similar air mass pathways throughout the day.

Exceptional is one afternoon flight segment (V2) during which the wind direction was inverted (direction between South and West). This probably caused the advection of aerosol with different properties as it was most likely influenced by anthropogenic

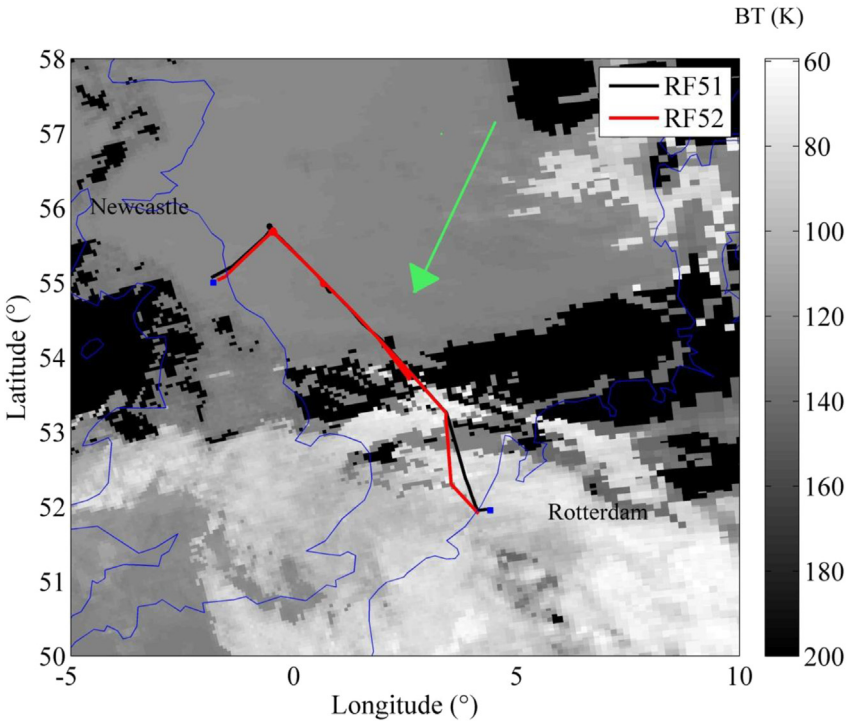


**Fig. 1.** Flight tracks of the two EUCAARI/IMPACT research flights (RF51 and RF52) performed on 15 May 2008 from Rotterdam (Netherlands) to Newcastle (United Kingdom) in the morning and subsequent return flight in the afternoon. The grayscale represents the brightness temperature from the MODIS-AQUA data for 15th May 2008 at 13:00. The green arrow illustrates the prevailing wind direction (see Fig. 5 and Fig. 6 for more details). (For interpretation of the references to color in this figure legend, the reader is referred to the web version of this article.)

emissions. Therefore, the flight segment V2 cannot be used to study interactions between aerosol and clouds in the main flow from North-East. As this episode of changed wind conditions during V2 was locally and temporarily very limited (i.e. ∼10 km of flight distance), this is not captured by these micro-scale features resolved by the FLEXPART tool.

The equivalent potential temperature ($\theta$e) can be used to distinguish two air masses with different origin and history (Colette et al., 2005; Sturman and McGowan, 1995) while the virtual potential temperature ($\theta$v) can be used to determine the buoyancy (Tables 2 and 3). As $\theta$e is a conservative parameter via adiabatic processes it allows evaluating air masses with respect to their state of mixture. In our case, it can be assumed that an identical $\theta$e indicates air masses with almost identical origin, identical strength of processing and particularly often homogeneously mixed conditions inside the air parcel. In our study, the comparison of $\theta$e at different altitudes (below 600 m and above 1000 m [asl]), shows significant differences (>5K in average), suggesting differences in air mass history and notably in their gaseous and aerosol concentrations and composition. Two principal aerosol layers are distinguished here that correspond to the boundary layer and the free troposphere. In the boundary layer, a rather stable $\theta$e is observed, consistent with a well-mixed layer. Nevertheless, the aerosol number concentration profiles performed in the afternoon show a decoupling of the boundary layer as described in Fig. 3. The latter case can be explained by a smooth and light decoupling of the boundary layer due do precipitation evaporation. The analyzed air masses have similar recent history, and therefore most likely similar gaseous and aerosol composition, except for the region below the cloud during the afternoon flight. At higher levels (>1000 m [asl]), the measurement period with wind directions from South-West (V2, cf. previous section), the horizontal variability of $\theta$e is larger (25K and 14K for RF51 and RF52, respectively). These results suggest that air masses in the free troposphere are of different types concerning their aerosol composition, state of aerosol processing or grade of aging.

Given the agreement in wind directions as measured and simulated (FLEXPART results) and the consistency of the equivalent potential temperature, one can assume that air masses sampled within the BL, in the morning and in the afternoon, might have similar origin.

## 4. Results

The most important measurements for this study were those of particle number size distributions and aerosol chemical composition. Subsequently aerosol particle size spectra and chemical composition were analyzed at different locations, with respect to the cloud layer. The V segments are located more than 130 km away from the coasts (United Kingdom and Netherlands), thus in a certain distance away from the immediate continental sources. Ideally, a survey of the aerosol properties prior to the cloud formation would have been used as a reference for non cloud processed aerosol. Unfortunately, the aerosol measurements during clear sky periods were limited to the V segments which were then used as a reference for non-processed aerosol.

Different aerosol–cloud processes can be examinated using our data set. Based on the conceptual model of the atmosphere and cloud that was drawn in Fig. 3, we will estimate the effect of aerosol activation and subsequent cloud processing. Concretely, aerosol properties in the Sc-vicinity within the boundary layer will be compared with the residual aerosol properties inside clouds. The influence of cloud processing with subsequent precipitation scavenging (drizzle clouds) on aerosol particles is assessed by comparing boundary layer aerosol properties in

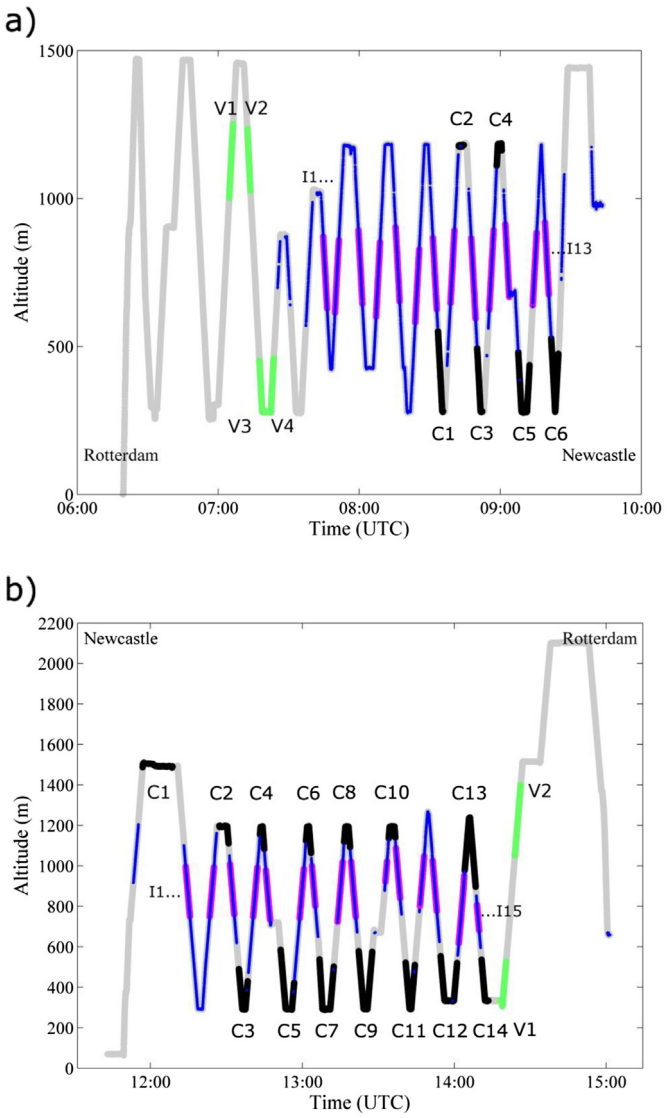


**Fig. 2.** Flight pattern and altitudes as a function of time for RF51 and RF52 from (a) Rotterdam to Newcastle and (b) the return flight on 15 May 2008. The blue color corresponds to the in-cloud periods. The measurements corresponding to in-cloud CVI measurements are illustrated by pink colors (I1—I13, and I1—I15, respectively). Green color represents flight segments during Sc-vicinity conditions, in the corresponding altitude range than measurements performed above/below (black) the stratocumulus cloud.

**Table 2**
Flight parameters during selected periods of interest of research flight RF51.

| Period label | Time interval in hh:mm | Altitude (m [asl]) | ATR-42 position relative to the cloud | $\theta$e in K | $\theta$v in K |
|---|---|---|---|---|---|
| V1 | 07:04–07:07 | 1130 | Sc-Vicinity | 236.5 | 293.8 |
| V2 | 07:12–07:14 | 1130 | Sc-Vicinity | 229.5 | 291.6 |
| V3 | 07:17–07:21 | 310 | Sc-Vicinity | 297.6 | 285.3 |
| V4 | 07:21–07:24 | 325 | Sc-Vicinity | 296.5 | 285.6 |
| C1 | 08:33–08:36 | 400 | Below Cloud | 297.8 | 283.7 |
| C2 | 08:42–08:44 | 1180 | Above Cloud | 280.1 | 290.8 |
| C3 | 08:50–08:52 | 355 | Below Cloud | 295.3 | 283.6 |
| C4 | 08:58–09:01 | 1175 | Above Cloud | 273.0 | 291.8 |
| C5 | 09:07–09:13 | 330 | Below Cloud | 299.4 | 283.6 |
| C6 | 09:21–09:25 | 390 | Below Cloud | 296.9 | 283.5 |

**Table 3**
Flight parameters during selected period of interest of research flight RF52.

| Period label | Time interval in hh:mm | Altitude (m [asl]) | ATR-42 position relative to the cloud | $\theta$e in K | $\theta$v in K |
|---|---|---|---|---|---|
| C1 | 11:56–12:08 | 1500 | Above Cloud | 265.4 | 293.1 |
| C2 | 12:27–12:30 | 1190 | Above Cloud | 279.6 | 291.7 |
| C3 | 12:35–12:38 | 350 | Below Cloud | 297.7 | 283.6 |
| C4 | 12:43–12:45 | 1170 | Above Cloud | 276.7 | 290.6 |
| C5 | 12:51–12:57 | 360 | Below Cloud | 297.1 | 283.5 |
| C6 | 13:01–13:03 | 1160 | Above Cloud | 272.6 | 290.8 |
| C7 | 13:07–13:12 | 345 | Below Cloud | 299.5 | 283.8 |
| C8 | 13:16–13:19 | 1180 | Above Cloud | 273.4 | 290.9 |
| C9 | 13:22–13:27 | 395 | Below Cloud | 296.6 | 283.9 |
| C10 | 13:34–13:37 | 1190 | Above Cloud | 272.9 | 291.0 |
| C11 | 13:41–13:44 | 385 | Below Cloud | 300.0 | 283.7 |
| C12 | 13:54–14:01 | 380 | Below Cloud | 300.6 | 284.3 |
| C13 | 14:04–14:08 | 1100 | Above Cloud | 236.5 | 291.6 |
| C14 | 14:11-14:21 | 370 | Below Cloud | 299.3 | 284.4 |
| V1 | 14:17–14:20 | 375 | Sc-vicinity | 299.9 | 284.7 |
| V2 | 14:23–14:26 | 1220 | Sc-vicinity | 239.3 | 293.7 |

the Sc-vicinity and immediately underneath the cloud layer (Fig. 2) at comparable altitudes. Because of the drizzle evaporation level and the resulting BL decoupling, the measurements performed during the afternoon (RF52) are not representative of one single layer. Thus, only the morning flight (RF51) measurements were conducive to study the influence of cloud and aerosol interactions.

### 4.1. Aerosol particle size distributions

The number size distributions were measured continuously during each flight and were averaged over specific periods (see Tables 2 and 3 as well as Fig. 2 for the predefined periods), in order to produce a mean particle number size distribution for each period. Subsequently mean volume size distributions were calculated from the mean number size distributions. The mean (number and volume) size distributions were fitted by using multi-modal log-normal distributions. Herein, a maximum of four modes was employed to describe the number distributions with sufficient

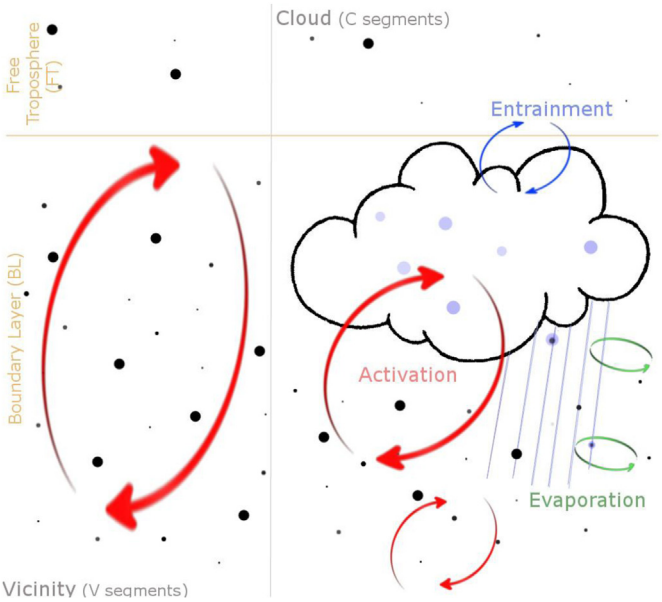


**Fig. 3.** Conceptual model of the structure of the lower troposphere for cloud free condition (Vicinity) and during the presence of a precipitating stratocumulus (Cloud).

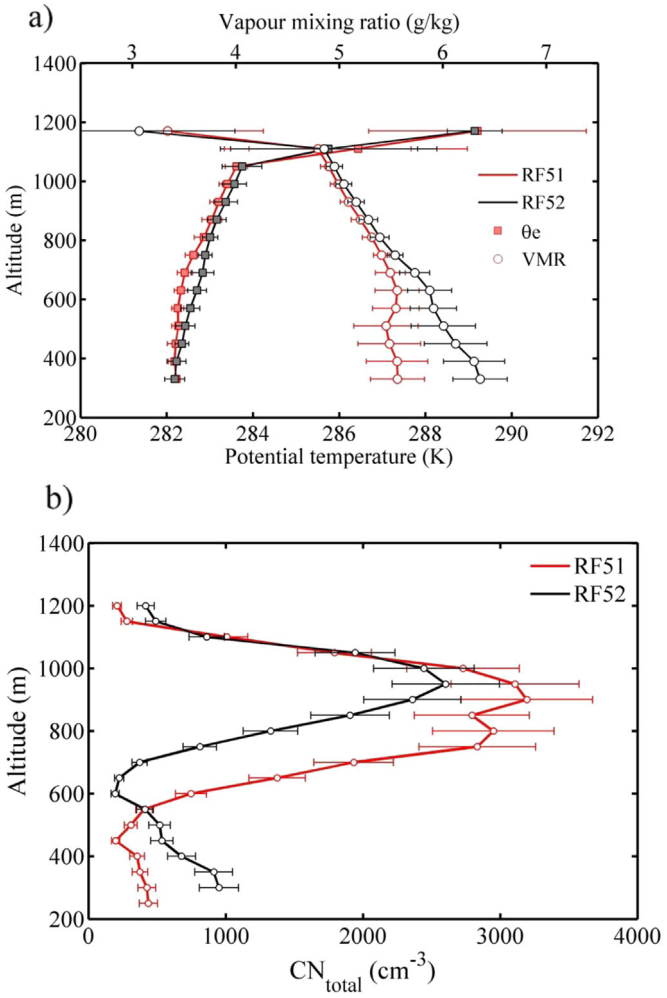


**Fig. 4.** Potential temperature and the vapor mixing ratio (a) and aerosol total number concentration (b) measured by a rosemount sensor, a dew point hygrometer and a particle counter (CPC-3010) during the research flight performed on the 15th May morning (RF51, red lines) and afternoon (RF52, black lines) as a function of altitude. The errorbars correspond to the 25th and 75th percentiles. (For interpretation of the references to color in this figure legend, the reader is referred to the web version of this article.)

detail. The parameters of each mode of the log-normal fit (number concentration, median diameter and geometric standard deviation) are shown in Table 4 (RF51) and in Table 5 (RF52), respectively. These fitted number size distributions are graphically presented in Fig. 7.

Aitken ($D < 0.1$ μm) and accumulation ($0.1 < D < 0.5$ μm) modes were identified in the boundary layer and in the free troposphere. The size distribution characteristics varied significantly as a function of sampling period and sampling altitude.

Looking first at research flight RF51 (Fig. 7a), a comparison of the averaged number size distributions for each period reveals significant differences, consistent with the presence of two distinct air mass layers (also seen from differences in the virtual and equivalent potential temperature):

a) Boundary layer (all segments below the temperature inversion altitude) in the vicinity of clouds (V segments), where the SMPS measured aerosol size distribution is clearly bimodal with distinct Aitken and accumulation particle modes. In between these two modes there is a pronounced minimum, known as the 'Hoppel minimum' (Hoppel et al., 1994, 1986) and potentially related to in-cloud aerosol processing and activation processes, principally observed between 70 and 90 nm. This diameter range corresponds to an effective maximum supersaturation (Fitzgerald et al., 1998; Feingold et al., 1996) achieved in this stratocumulus. The Hoppel minimum is more apparent during the 'below-cloud' cases (C segments) compared to corresponding altitudes of Sc-vicinity periods. Below the precipitating cloud, an additional modification of the aerosol size distribution is likely due to collision scavenging of aerosols from drizzle droplets. The mean diameter of the accumulation mode of aerosol particles reached 223 nm below the cloud (C segments) while the mean diameter was ranged at about 177 nm at corresponding altitudes within Sc-vicinity periods (V segments).

The number concentrations of the Aitken and the accumulation particle modes measured below the cloud are decreasing in comparison to the measurements performed in the cloud vicinity. The particle losses are estimated to range at 16% for the Aitken modes (<50 nm) and more than 42% for the accumulation mode (>100 nm). Indeed, the geometric standard deviations of the fitted accumulation mode are small (<1.44) and decrease below the cloud layer. Interestingly, the larger particle (>250 nm) concentrations are similar during both periods. Based on explicit calculations of the collision efficiency between a raindrop and aerosol particles, Andronache (2003) show that the mean mass scavenging coefficient has a minimum ($1.2 \cdot 10^{-3}$ $h^{-1}$) for aerosol particles with a geometric mean diameter between 40 and 70 nm and the same coefficient ranges three order of magnitude higher (0.35–1 $h^{-1}$) than this minimum for larger aerosol particles ($D > 250$ nm). Thus, the decrease of the aerosol (40–200 nm) number concentration is most likely affected due to in-cloud transformation processes (droplet collision/coalescence). However, these processes would have led to an increase of the larger particles number concentration, which is not observed, possibly due to drizzle wash out from the sampled layer.

b) Free troposphere (all segments above the temperature inversion altitude): Compared to the boundary layer, in the free troposphere the size distribution modes move from 147 nm to 234 nm (periods V1 and V2) during Sc-vicinity periods to a single mode distribution at 88.3 nm at corresponding above-cloud altitudes. The entrainment of air masses into the cloud layer seems to have an effective impact within a layer of 200 m above the cloud top. Thus, entrainment of dry air into the cloud might lead to the trapping of larger particles ($D > 250$ nm). Indeed, in the layer just above the cloud, larger particles could be trapped in the cloud layer due to activation, rain out and collision process (Jiang et al., 2002). This hypothesis will be reinforced by the analysis of the total mass concentration measured by the cToF-AMS (Section 4.2).

The observations that were made during the afternoon flight RF52 (Fig. 7b) were similar. The measurement results show less accumulation mode particles above the cloud layer and enhanced number and larger sizes of accumulation mode particles below the cloud layer as compared to the cloud free conditions (cloud vicinity). A nucleation mode appears to be present below the cloud base. Usually, the presence of clouds likely interrupts the nucleation process through the scavenging of condensable vapors and/or pre-existing ion-clusters of gaseous precursors by cloud droplets (Venzac et al., 2007; Boulon et al., 2011). Measurements of gaseous precursors were not performed aboard the ATR-42 during EUCAARI which limits the exploration of the process that would lead to this

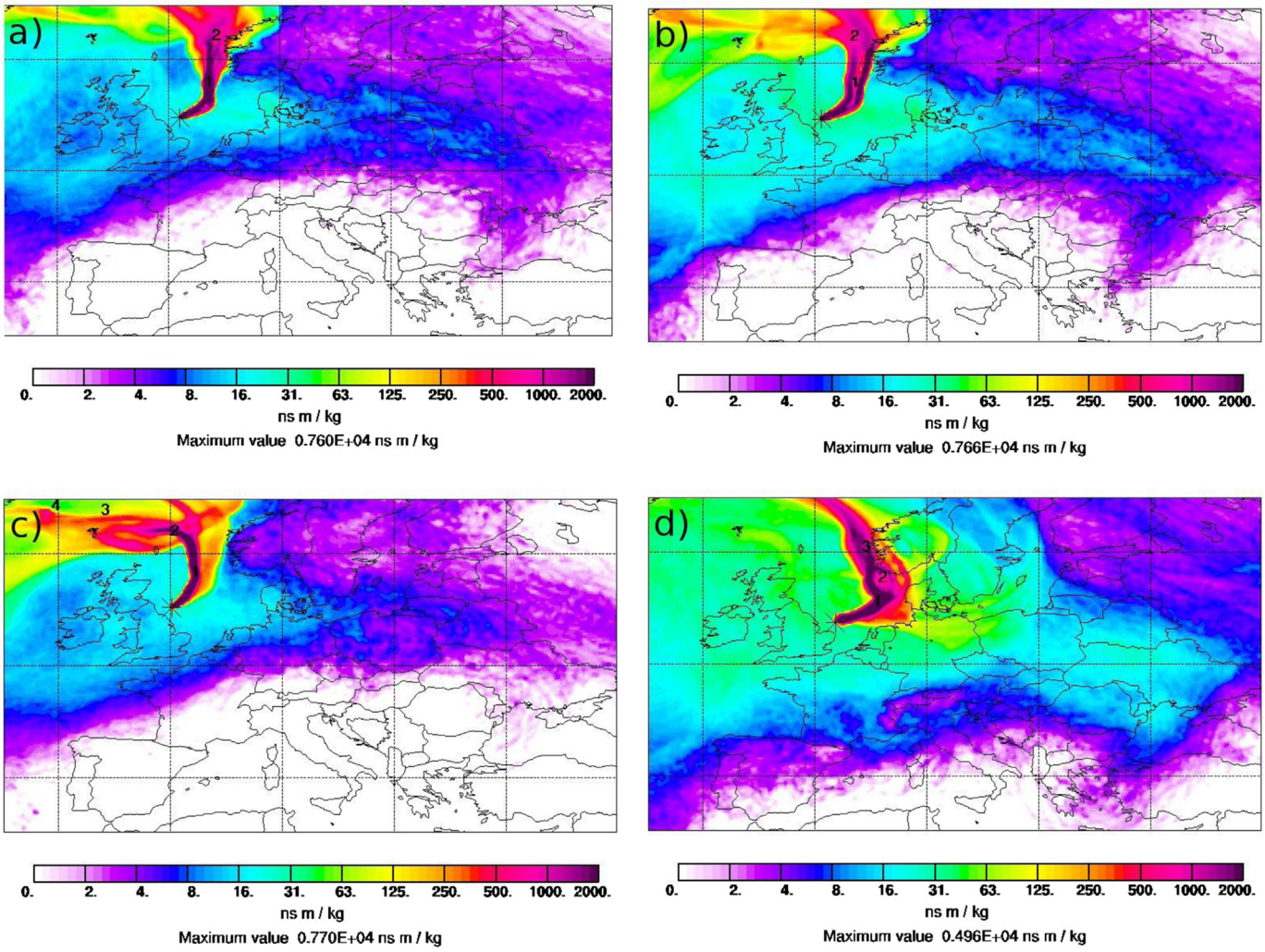


**Fig. 5.** Column integrated emission sensitivities obtained from the 3-day backward simulation with FLEXPART along the ATR-42 flight track on 15 May, 2008 at 07:29 UTC at the altitude of 403 m (a), 09:02 UTC at 901 m (b), 12:21 UTC at 349 m (c), and 14:08 UTC at 920 m (d). Numbers represent the days backward in time.

particle formation event. Moreover, below the cloud, during the morning as well as the afternoon, a third particle mode is observed and centered at a diameter of 120 nm. Despite the cloud/aerosol interactions, this aerosol mode remains the same throughout the day. This result highlights an external mixing of particles with a potentially hydrophobic aerosol population.

### *4.2. Mass concentrations*

#### *4.2.1. 'Near-cloud' measurements*

Fig. 8 show the aerosol mass concentrations measured by the cToF-AMS during the morning (RF51) and the afternoon (RF52) flights. The mass concentrations of non-refractory particles are

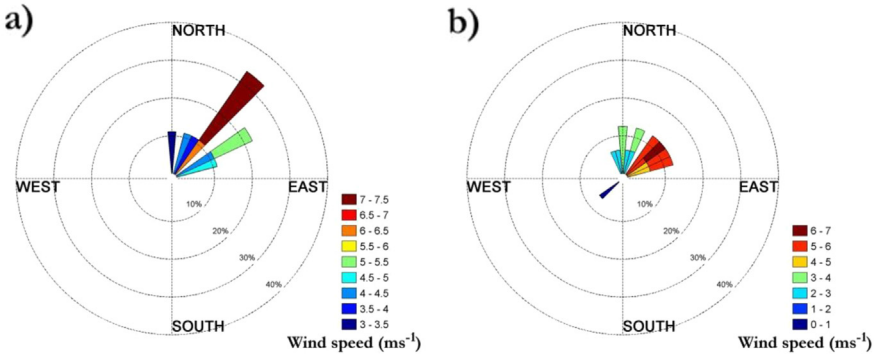


**Fig. 6.** Wind roses calculated for constant altitude legs, in the boundary layer and in the free troposphere, for the morning flight (RF51, a) and the afternoon flight (RF52, b). The colorscale indicates wind speed (ie. between 0 and 10 m $s^{-1}$). The bar length correspond to the occurrence frequency of respective wind direction throughout each episode.

**Table 4**
Log-normal characteristics of the number size distributions shown in Fig. 7a distinguishing two altitude layers, the Boundary Layer (BL) and the Free Troposphere (FT). $C$ represents the concentration of the particle mode ($cm^{-3}$), $\sigma$ the standard deviation of the number concentration ($cm^{-3}$), and $D_{med}$ is the median diameter (nm), NA stands for not applicable.

| | | Sc-vicinity | | | Below/Above Sc | | |
|---|---|---|---|---|---|---|---|
| | | $C$ ($cm^{-3}$) | $\sigma$ | $D_{med}$ (nm) | $C$ ($cm^{-3}$) | $\sigma$ | $D_{med}$ (nm) |
| BL | Mode 1 | 104 | 1.3 | 35 | 275 | 1.29 | 38 |
| | Mode 2 | 224 | 1.24 | 47 | 33 | 1.14 | 120 |
| | Mode 3 | 443 | 1.44 | 176.9 | 223 | 1.32 | 223 |
| FT | Mode 1 | 392 | 1.34 | 48.3 | 316 | 1.16 | 26.9 |
| | Mode 2 | 451 | 1.4 | 146.6 | 107 | 2.0 | 88.3 |
| | Mode 3 | 96 | 1.47 | 234 | NA | NA | NA |

presented for the different segments in the cloud vicinity and above/below the stratocumulus layer for both layers (BL, FT). Number concentration gradients observed on the aerosol size distributions (SMPS) are coherent with the gradients observed on the aerosol mass concentrations (cToF-AMS).

In the boundary layer (<1000 m [asl]), the median mass concentrations are lower than 12.1 μg.$m^{-3}$. During the morning flight (RF51), the observed mass concentrations decreased as the aircraft approaches the cloud: 11.66 ± 0.3 μg $m^{-3}$ in the cloud vicinity and 6.57 ± 0.3 μg $m^{-3}$ below the cloud base. This mass concentration decrease was even more pronounced during the afternoon flight (RF52), probably due to a longer exposure period for interaction with cloud elements, and then may have increased the wash out and the entrainment/activation below the cloud. The averaged mass concentrations during the afternoon are about 12.08 μg $m^{-3}$ in the cloud vicinity and about 5.12 ± 0.2 μg $m^{-3}$ below the cloud base.

As described before, the layer immediately above the cloud layer corresponds to an inversion layer characterized by a mixing of free tropospheric air with cloud depleted air. The mixing of these two layers causes a dilution of the aerosol concentration. Due to similar air mass transport (Section 3.2), we can assume similar aerosol mass concentrations within the FT during cloud free periods and above the cloud inversion layer (8.84 μg $m^{-3}$ and 4.45 μg $m^{-3}$, respectively during the morning and in the afternoon flights). In this inversion layer, the aerosol mass concentrations are lower (<1.16 μg $m^{-3}$ and <2.62 μg $m^{-3}$ during the morning and the afternoon flights, respectively). During the morning flight, the aerosol mass concentrations within the inversion layer are 3 times lower than measured inside the cloud (3.92 μg $m^{-3}$ and 2.78 μg $m^{-3}$ respectively during the morning and the afternoon flights). Aerosol removal process would likely suggests the loss of aerosol mass concentration in the inversion layer. The entrainment at the cloud top, through the activation of the larger particle and the sedimentation of the cloud droplets, may lead larger particles getting trapped. The decrease of aerosol mass concentration above the cloud most likely due to entrainment of free tropospheric (and cleaner) air masses and is consistent with previous airborne observations (Hoppel et al., 1994; Hegg et al., 1990).

During the afternoon flight, the vertical gradient of the aerosol mass concentrations is not as expressed as the one observed in the morning. Moreover, a nucleation mode of particles is observed in this inversion layer. The low aerosol mass concentrations and high concentration of gaseous nucleation precursors – likely close to saturation due to low ambient air temperatures – make the conditions more favorable for new particle formation events.

**Table 5**
Log-normal characteristics of the number size distributions shown in Fig. 7b distinguishing two altitude layers, the Boundary Layer (BL) and the Free Troposphere (FT). $C$ represents the concentration of the particle mode ($cm^{-3}$), $\sigma$ is the standard deviation of the number concentration ($cm^{-3}$) and $D_{med}$ is the median diameter (nm), NA stands for not applicable.

| | | Sc-vicinity | | | Below/Above Sc | | |
|---|---|---|---|---|---|---|---|
| | | $C$ ($cm^{-3}$) | $\sigma$ | $D_{med}$ (nm) | $C$ ($cm^{-3}$) | $\sigma$ | $D_{med}$ (nm) |
| BL | Mode 1 | 490 | 1.34 | 53 | 130 | 1.25 | 21.2 |
| | Mode 2 | 444 | 1.45 | 173.5 | 246 | 1.34 | 45.7 |
| | Mode 3 | NA | NA | NA | 37 | 1.19 | 131 |
| | Mode 4 | NA | NA | NA | 183 | 1.34 | 242.2 |
| FT | Mode 1 | 89 | 1.33 | 46.3 | 174 | 1.41 | 35.4 |
| | Mode 2 | 58 | 1.31 | 98.9 | 59 | 1.26 | 109.4 |
| | Mode 3 | 62 | 1.88 | 137 | 99 | 1.41 | 240 |

#### 4.2.2. 'In cloud' measurements

To investigate the characteristics of aerosol particle activation into cloud droplets, cToF-AMS analyses of the aerosol material incorporated in cloud elements were performed. To study the aerosol incorporated in cloud droplets, the CVI sampling technology was utilized. The combination of the Aerodyne aerosol mass spectrometer with two main aerosol inlets (CAI and CVI inlets) has proven to be a valuable tool for measuring the ambient aerosol and cloud droplet residuals (Drewnick et al., 2007). The average mass concentrations of aerosol particulate matter incorporated in the liquid phase of the stratocumulus cloud layer were found to be 3.92 ± 1.09 μg $m^{-3}$ and 2.78 ± 1.15 μg $m^{-3}$ (one standard deviation) during the morning and the afternoon flights, respectively. The ratio of the activated aerosol mass concentration to the aerosol mass concentration measured within the BL in the cloud vicinity is a rough estimation of the activated aerosol fraction. As stated before, the collection efficiency to correct the AMS mass concentrations are calculated using the same procedure during cloud and clear sky periods. In the morning, the activated aerosol fraction is about 33% while in the afternoon the fraction decreased to 23%.

### 4.3. Chemical composition

#### 4.3.1. 'Cloud-free' measurements

Averages of the fractional chemical composition of aerosol particles measured with the cToF-AMS for all flight segments are presented in Fig. 9 for the morning flight (RF51) and in Fig. 10 for the afternoon flight (RF52), respectively. In both figures, the top panel corresponds to the relative chemical composition of measurements in the free troposphere, whereas the bottom figure corresponds to measurements in the boundary layer. For both layers, the exact positions of measurements during the cloud vicinity and below/above cloud segments are represented by the color code.

During the morning flight (RF51) in the FT, the fraction of organic aerosol material decreased during transits from the cloud vicinity into above/below cloud layers, while the fractions of sulfate and ammonium increased. The low fraction of organic components above the cloud system may be related to the change of air mass types, as shown with the equivalent potential temperatures (see Section 3.2), and may be a consequence of the entrainment of organic aerosol into the cloud layer and its immediate activation in the vapor saturated environment. In general, the fraction of sulfate species in the aerosol is dominant (>45%) except for the V2 segment when the organic fraction was by a factor of two larger compared to sulfate (aerosol from anthropogenic sources were found in this flight segment).

Below the cloud base in comparison to the cloud vicinity, the relative fractions of organics are small (<15%) while the fractions of ammonium and sulfate are high, in the morning as well as in the afternoon. The enhancement of sulfate and ammonium might be a

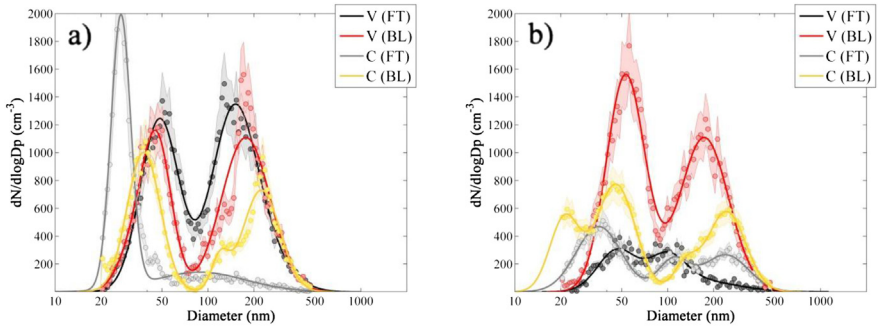


**Fig. 7.** Averaged number size distributions of particles observed during RF51 on May 15th in the morning (a) and during RF52 in the afternoon of the same day (b). Bright (dark) lines represent measurements performed in the boundary layer (free troposphere). Red and black colors correspond to Sc-vicinity measurements (V segments) and orange and gray colors correspond to above and below the stratocumulus cloud system (C segments).

consequence of two different processes: (i) by evaporation of cloud droplets containing a nuclei that consist made of inorganic material (linked to a preferential activation of inorganic species) or (ii) by aqueous production of sulfate (Hegg and Hobbs, 1982; Joos and Baltensperger, 1991).

*4.3.2. 'In-cloud' measurements*

The average fractional contribution of cloud residual aerosol chemical compounds for each in-cloud flight segment (700–1000 m altitude), are presented in Fig. 11 (a) for the morning and Fig. 11 (b) for the afternoon flight, respectively. More than 68% of the mass concentration of non-refractory aerosol is composed of sulfate and organic components for all samples. The third most important compound is nitrate with relative abundance of more than 8%.

A comparison of the chemical composition of non processed aerosol (V segments) with the material incorporated in the liquid phase yields some interesting results (Table 6). The sulfate fractions, observed during 'in-cloud' conditions, are 44% and 51% while in the Sc-vicinity in the BL, it is 60% and 47% during the morning and the afternoon flight, respectively. Moreover, the absolute concentration of sulfate, during the afternoon flight, is two times larger during the Sc-vicinity period in the BL (2.67 ± 0.8 μg m$^{-3}$) than during in cloud period (1.45 ± 0.58 μg m$^{-3}$). The ratio of 'in-cloud' to 'vicinity' mass concentration is a measure of the Efficiency of Activation and in-cloud Production (EAP). The size distributions for each compound are not available, thus the assumption of an internal mixing has to be made. As size distributions of nitrate and sulfate submicron aerosol are generally similar (Wall et al., 1988; Jaffrezo et al., 2005; Zhang et al., 2005; Stroud et al., 2007; Plaza et al., 2011) while the size distributions of organic submicron aerosol are generally centered to smaller size (Sun et al., 2010; Jimenez et al., 2003), only the nitrate and sulfate EAP will be compared.

The sulfate EAP is low (24%) compared to measurements previously shown in the literature (Hinds, 1998; Vocourt, 2002; Sellegri et al., 2003). The cloud residual concentrations of nitrate compounds (0.55 ± 0.10 μg m$^{-3}$) are slightly larger than those measured within Sc-vicinity segments in the BL (0.32 ± 0.05 μg m$^{-3}$) during the morning flight. The higher nitrate concentrations, found in cloud residual (EAP = 168%), is consistent with results from Drewnick et al. (2007) and is suggesting that some nitrate is also produced in cloud droplets or by scavenging of ammonia vapor (Leaitch et al., 1986). The organics absolute mass concentrations are higher in the dry phase (3.355 ± 0.14 μg cm$^{-3}$ during the morning flight) than in the liquid residual phase (0.938 ± 0.4 μg m$^{-3}$ during the morning flight).

The morning and afternoon flights comparison highlights different tendencies (Table 4). A major difference of absolute and relative concentrations is observed for chloride, as we compare cloud-free and in-cloud concentrations. Indeed, during the cloud vicinity periods, the chloride fraction remains on average smaller than 1% (morning: 0.100 ± 0.06 μg m$^{-3}$, afternoon: 0.020 ± 0.01 μg m$^{-3}$). During 'in-cloud' periods, the chloride fractions are on average between 1 and 10% (morning: 0.233 ± 0.1 μg m$^{-3}$, afternoon: 0.065 ± 0.04 μg m$^{-3}$). Thus, the chloride fractions are larger in cloud residuals than in dry aerosol particles, suggesting that most of the chloride mass is found in the largest (thus potentially cloud forming) particles.

Although it cannot be proven, the assumption that sea salt aerosol and gaseous organic-chloride species emitted from the sea surface, are present in the BL over the North Sea appears to be plausible. These species are per-se hardly or not detectable by a cToF-AMS. Sodium chloride itself is an excellent CCN due to its strongly hygroscopic character and organic chloride compounds (e.g. methyl chloride) are most likely incorporated by cloud elements as well. It is also conceivable that in the cloud element residuals, e.g., inorganic chloride aerosol species such as hydrogen chloride (HCl) or ammonium chloride ($NH_4Cl$) are present, or that complex organic chloride compounds are bonded to other vaporizable cloud element residuals.

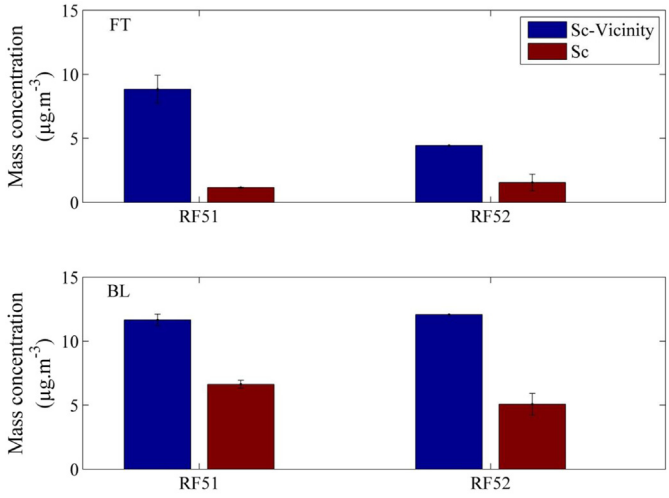


**Fig. 8.** Averaged particle mass concentrations from cToF-AMS measurements for RF51, during Sc-vicinity segments and below/above the stratocumulus cloud. The upper panel corresponds to the free troposphere measurements (1150 m [asl] for RF51 and 1250 m [asl] for RF52); the bottom panel corresponds to boundary layer measurements (330 m [asl] for RF51 and 350 m [asl] for RF52).

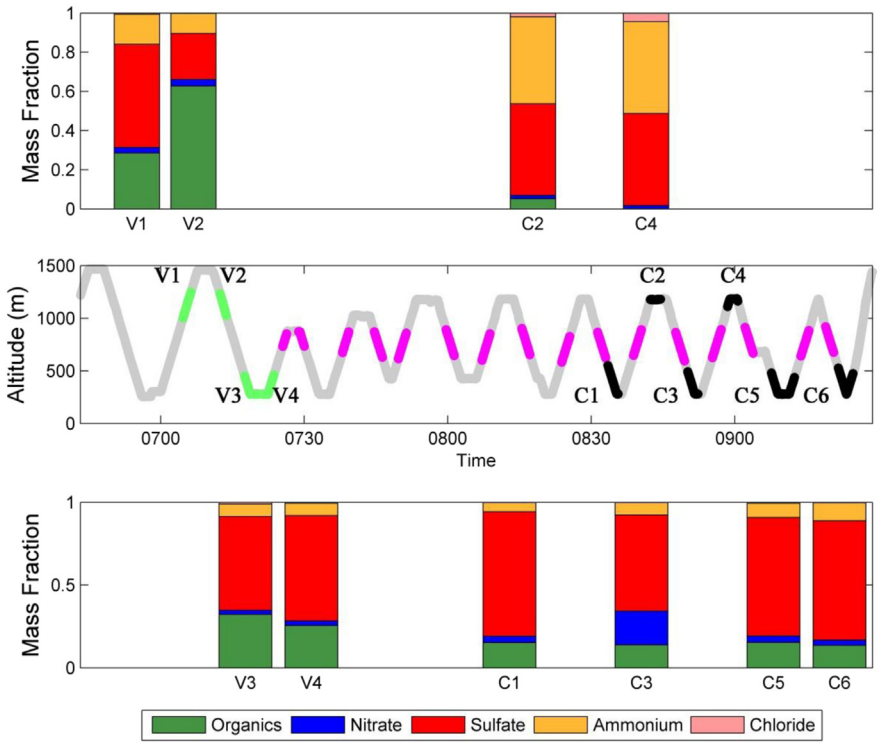


**Fig. 9.** Averaged particle chemical composition from cToF-AMS measurements for RF51, during Sc-vicinity (V1−V4), and below/above the stratocumulus layer (C1−C6). Five chemical compounds are shown: Organics, Nitrate, Sulfate, Ammonium and Chloride. The upper panel corresponds to 1150 m [asl] flight altitude, the bottom panel corresponds to 350 m [asl] flight altitude.

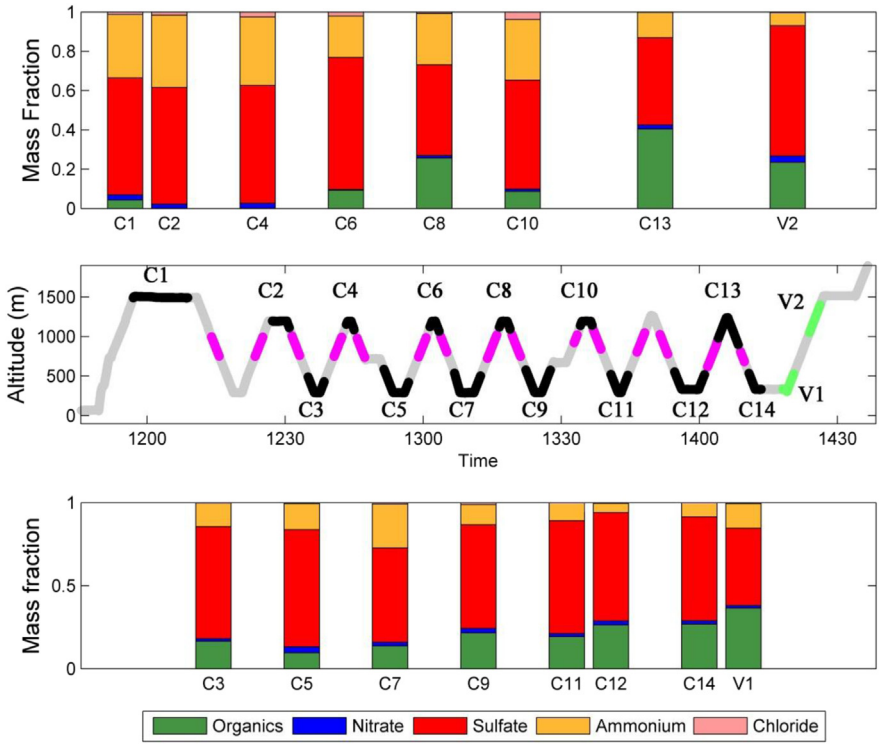


**Fig. 10.** Averaged particle chemical composition from cToF-AMS data for RF52, during Sc-vicinity (V1−V2), and below/above the stratocumulus layer (C1−C14). The upper panel corresponds to 1250 m [asl] flight altitude, the bottom panel corresponds to 350 m [asl] flight altitude.

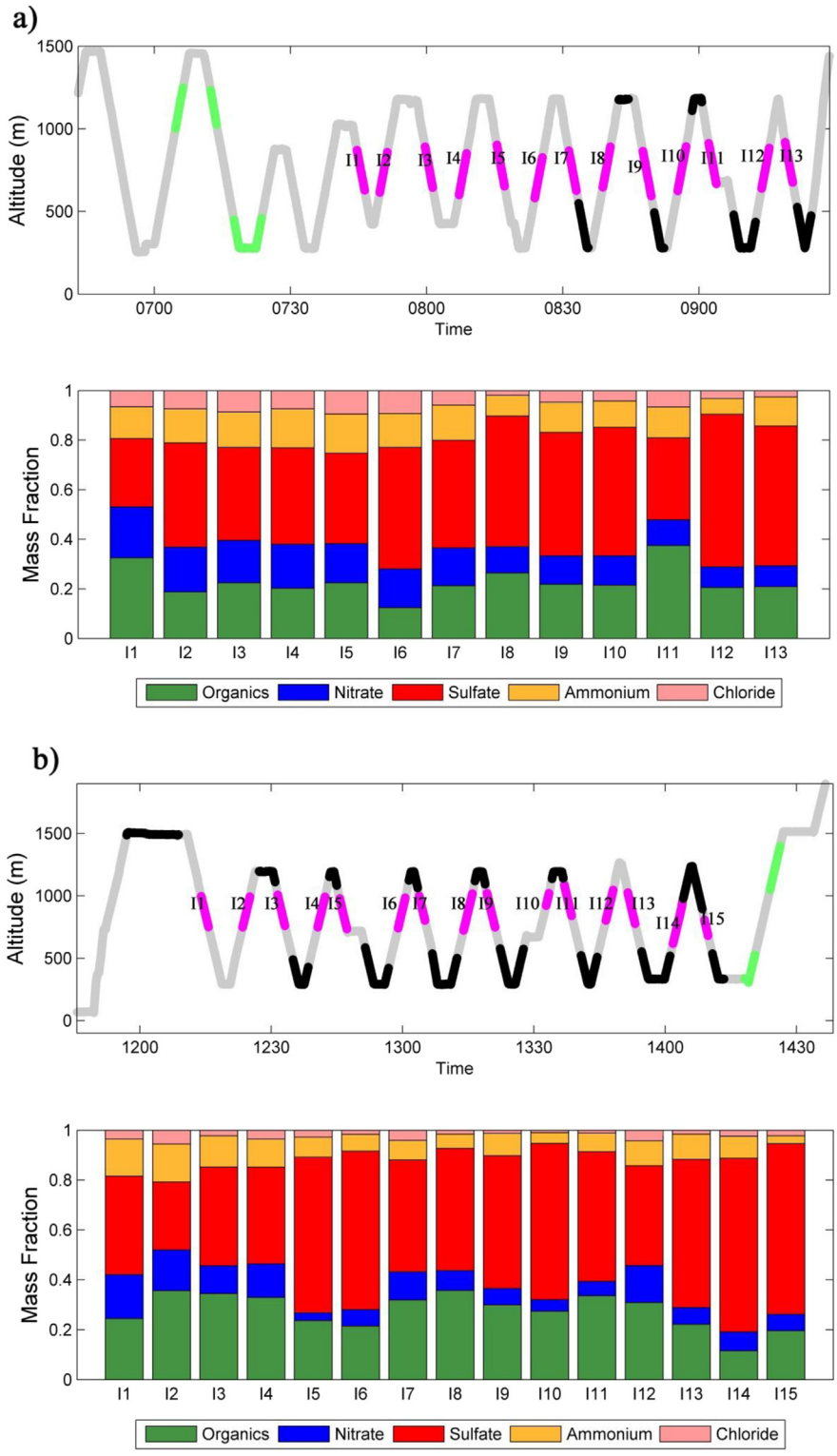


**Fig. 11.** Averaged particle chemical composition during in cloud conditions (I1–I13 and I1–I15, respectively) for research flights RF51 (a) and RF52 (b). The mass fraction figures correspond to about 800 m [asl] flight altitude.

## 5. Summary and conclusions

Within the framework of the EUCAARI intensive observation period, size distributions, mass concentrations, and chemical composition of aerosol particles have been measured during two research flights in order to study the aerosol–cloud interactions within an extended stratiform cloud system. On 15 May 2008, a stratocumulus cloud deck formed over the North Sea, between Rotterdam (Netherlands) and Newcastle (United Kingdom). The ATR-42 performed two flights with an outgoing flight during the morning (RF51) and a return flight during the afternoon (RF52). In order to characterize the evolution of aerosol particles due to cloud

**Table 6**
Averaged mass concentration of organic, nitrate, sulfate, ammonium, chloride in the vicinity of the cloud and in the cloud during the morning (RF51) and the afternoon flight (RF52). Efficiency of Activation and in-cloud Production (EAP) is the estimated percentage of each component activated and produced in the cloud (see text for more details).

| | | Organics ($\mu g\ m^{-3}$) | Nitrate ($\mu g\ m^{-3}$) | Sulfate ($\mu g\ m^{-3}$) | Ammonium ($\mu g\ m^{-3}$) | Chloride ($\mu g\ m^{-3}$) |
|---|---|---|---|---|---|---|
| RF-51 | Vicinity BL | 3355 | 0.320 | 7025 | 0.865 | 0.100 |
| | In cloud | 0.937 | 0.540 | 1704 | 0.490 | 0.233 |
| | EAP (%) | 28 | 169 | 24 | 57 | 233 |
| RF-52 | Vicinity BL | 1624 | 0.070 | 2074 | 0.658 | 0.027 |
| | In cloud | 0.817 | 0.268 | 1371 | 0.251 | 0.071 |
| | EAP (%) | 50 | 383 | 66 | 38 | 263 |

processes we compared particle properties within the cloud vicinity segments to below/above as well as in cloud segments. Fig. 12 and Fig. 13 summarize the measured mass concentrations, the chemical composition of particles observed during the cloud vicinity, below/above stratocumulus layer, as well as in-cloud for the morning and the afternoon flights, respectively. The analysis of the aerosol and thermodynamic profiles highlight the presence of three distinct layers: between 0–450 m [asl] (corresponding to the part of the boundary layer connected to the surface), 450–600 m [asl] (corresponding to the part of boundary layer connected to the cloud) and 600–1200 m [asl](corresponding to the free troposphere explored by the ATR-42 during the two flights). The analysis of wind directions observed during the morning and the afternoon flights and model calculations concerning the air mass transport paths reveals that observed air masses are originating from North-East with respect to the flight pattern.

The number size distributions show that Aitken ($D < 0.1\ \mu m$) and accumulation ($0.1 < D < 0.5\ \mu m$) modes were present in both layers. The presence of particles from a nucleation mode ($D < 0.02\ \mu m$) was also observed above the cloud layer during the morning flight and below the cloud layer during the afternoon flight. The averaged size distributions observed below the cloud layer highlight a pronounced minimum between the two principal modes, known as the 'Hoppel minimum' (Hoppel et al., 1994), of the bimodal aerosol size distribution observed during stratocumulus-vicinity period. Since bi-modal distributions have been shown to result from cloud processing (Hoppel et al., 1994; Saxena, 1996; Clarke et al., 1996; Weber and McMurry, 1996), we can conclude that this pronounced bimodal shape is due to (1) activation, (2) addition of mass to cloud droplets.

Moreover, the concentration of particles in the accumulation mode size range decreases above and below the cloud layer as compared to the cloud vicinity periods, consistent with the simultaneous decrease of mass concentrations shown in Figs. 12 and 13. The loss of particulate mass above the cloud may be related to entrainment of particles into the cloud layer and immediate activation of those, or collision/coalescence and wash out.

Finally, Figs. 12 and 13 highlight a strong dependence of the aerosol chemical composition on the observation location (vicinity or below/above the cloud). The fraction of nitrate compounds increases in the cloud residual phase, while the fraction of sulfate decreases. Interestingly, the mass concentrations of nitrate are larger in the cloud residual in comparison to cloud vicinity periods (by a factor of 1.7–3.8 in the morning and in the afternoon respectively) suggesting in cloud production of nitrate or ammonia vapor uptake artificially increasing the EAP of nitrate (Leriche et al., 2007).

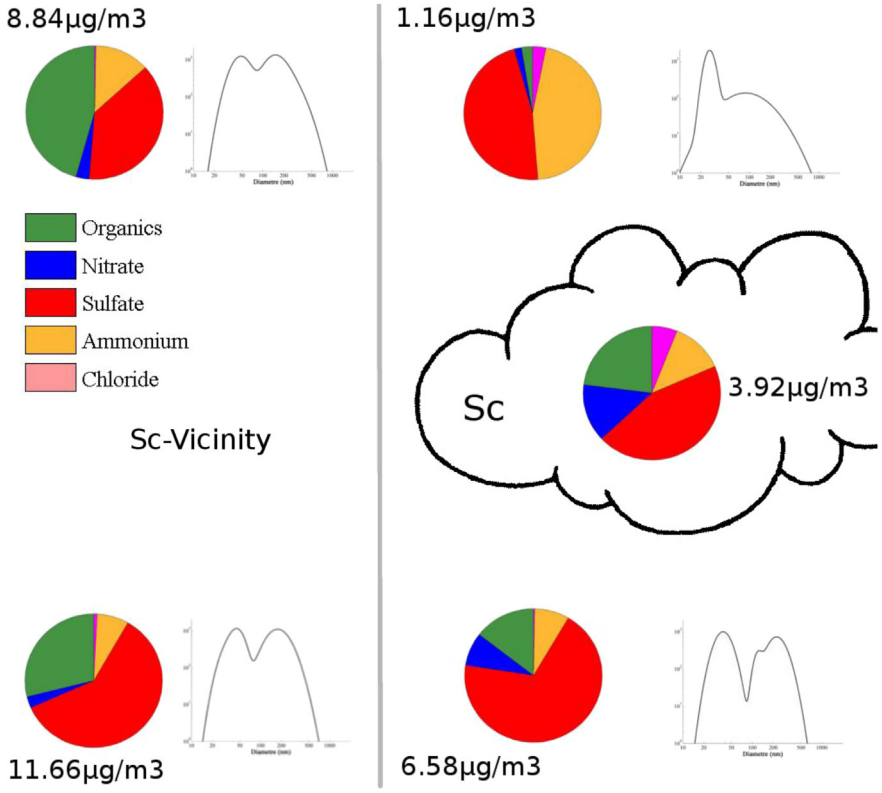


**Fig. 12.** Summary of particle chemical composition from cToF-AMS measurements for research flight RF51 during Sc-vicinity, below/above stratocumulus layer, as well as in-cloud analysis from CVI inlet at different altitude levels (lower layer at 300–600 m [asl], cloud level 600–1000 m [asl], and upper layer at 1000–1500 m [asl]).

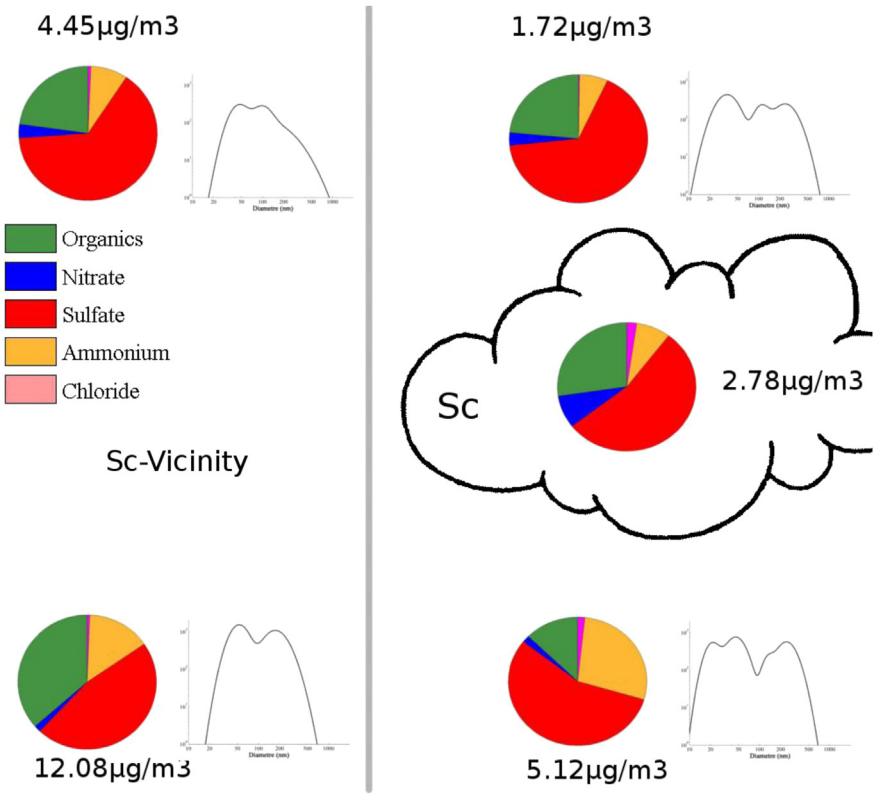


**Fig. 13.** Summary of particle chemical composition from cToF-AMS measurements for research flight RF52 during Sc-vicinity, below/above stratocumulus layer, as well as in-cloud analysis from CVI inlet at different altitude levels (lower layer at 300–600 m [asl], cloud level 600–1000 m [asl], and upper layer at 1000–1500 m [asl]).

In order to improve our knowledge on complex aerosol–cloud processes, this case study could be used by the modeling community as a reference for the conditions related to a precipitating stratiform cloud. The present study provides worthfull hints concerning possible improvements of the instrumentation and flight strategy of future airborne missions devoted to aerosol and cloud interactions. Indeed, the next studies should be able (i) to survey the aerosol properties prior to cloud formation, (ii) to focus on non precipitating cloud to simplify the analysis, (iii) to perform complete profiles from the lowest altitude level to the free troposphere, disconnected from the cloud top and (iv) to perform multiple missions to get statistically robust conclusions.

## Acknowledgments

This work has been partially funded by European Commission 6th Framework program project EUCAARI, contract no 036833-2 (EUCAARI), and by the French National Research Agency (ANR) under the AEROCLOUD program, contract no 06-BLAN-0209. Suzanne Crumeyrolle has been supported by CNRS fellowship (contract n°167641). The authors wish to thank the SAFIRE (Service des Avions Français Instruments pour la Recherche en Environnement) for preparing and delivering the research aircraft (ATR-42).

## References

Adams, P.J., Seinfeld, J.H., 2002. Predicting global aerosol size distributions in general circulation models. J. Geophys. Res. 107 (D19), 4370. http://dx.doi.org/10.1029/2001JD001010.

Andrejczuk, M., Grabowski, W.W., Reisner, J., Gadian, A., 2010. Cloud–aerosol interactions for boundary layer stratocumulus in the Lagrangian Cloud Model. J. Geophys. Res. 115, D22214. http://dx.doi.org/10.1029/2010JD014248.

Andronache, C., 2003. Estimated variability of below-cloud aerosol removal by rainfall for observed aerosol size distributions. Atmos. Chem. Phys. 3, 131–143. http://www.atmos-chem-phys.net/3/131/2003/.

Bahreini, R., Dunlea, E.J., Matthew, B.M., Simons, C., Docherty, K.S., DeCarlo, P.F., Jimenez, J.L., Brock, C.A., Middlebrook, A.M., 2008. Design and operation of a pressure controlled inlet for airborne sampling with an aerodynamic aerosol lens. Aerosol Sci. Tech. 42 (6), 465–471.

Barth, M.C., Rasch, P.J., Kiehl, J.T., Benkovitz, C.M., Schwartz, S.E., 2000. Sulfur chemistry in the National Center for Atmospheric Research Community Climate Model: description, evaluation, features, and sensitivity to aqueous chemistry. J. Geophys. Res. 105 (D1), 1387–1415.

Boulon, J., Sellegri, K., Hervo, M., Picard, D., Pichon, J.-M., Fréville, P., Laj, P., 2011. Investigation of nucleation events vertical extent: a long term study at two different altitude sites. Atmos. Chem. Phys. 11, 5625–5639.

Bower, K.N., Choularton, T.W., Gallagher, M.W., Colvile, R.N., Wells, M., Beswick, K.M., Wiedensohler, A., Hansson, H.-C., Svenningsson, B., Swietlicki, E., Wendisch, M., Berner, A., Kruisz, C., Laj, P., Facchini, M.C., Fuzzi, S., Bizjak, M., Dollard, G., Jones, B., Acker, K., Wieprecht, W., Preiss, M., Sutton, M.A., Hargreaves, K.J., Storeton-West, R.L., Cape, J.N., Arends, B.G., 1997. Observation and modelling of the processing of aerosol by a hill cap cloud. Atmos. Environ. 31, 2527–2543.

Brenguier, J.-L., Burnet, F., Geoffroy, O., 2011. Cloud optical thickness and liquid water path – does the k coefficient vary with droplet concentration? Atmos. Chem. Phys. 11, 9771–9786 http://dx.doi.org/10.5194/acp-11-9771-2011.

Canagaratna, M.R., Jayne, J.T., Jimenez, J.L., Allan, J.D., Alfarra, M.R., Zhang, Q., Onasch, T.B., Drewnick, F., Coe, H., Middlebrook, A., Delia, A., Williams, L.R., Trimborn, A.M., Northway, M.J., DeCarlo, P.F., Kolb, C.E., Davidovits, P., Worsnop, D.R., 2007. Chemical and microphysical characterization of ambient aerosols with the aerodyne aerosol mass spectrometer. Mass Spectrom. Rev. 26, 185–222.

Clarke, A.D., Li, Z., Litchy, M., 1996. Aerosol dynamics in the equatorial Pacific marine boundary layer: microphysics, diurnal cycles and entrainment. Geophys. Res. Lett. 23 (7), 733–736. http://dx.doi.org/10.1029/96GL00778.

Colette, A., Ancellet, G., Borchi, F., 2005. Impact of vertical transport processes on the tropospheric ozone layering above Europe. Part I: Study of air mass origin using multivariate analysis, clustering and trajectories. Atmos. Environ. 39 (29), 5409–5422. ISSN 1352-2310, http://dx.doi.org.10.1016/j.atmosenv.2005.06.014.

Crosier, J., Allan, J.D., Coe, H., Bower, K.N., Formenti, P., Williams, P.I., 2007. Chemical composition of summertime aerosol in the Po-Valley (Italy), northern Adriatic and Black Sea. Q. J. R. Meteorol. Soc. 133 (S1), 61–75.

Crumeyrolle, S., Gomes, L., Tulet, P., Matsuki, A., Schwarzenboeck, A., Crahan, K., 2008. Increase of the aerosol hygroscopicity by cloud processing in a mesoscale

convective system: a case study from the AMMA campaign. Atmos. Chem. Phys. 8, 6907–6924. http://dx.doi.org/10.5194/acp-8-6907-2008.
Crumeyrolle, S., Manninen, H.E., Sellegri, K., Roberts, G., Gomes, L., Kulmala, M., Weigel, R., Laj, P., Schwarzenboeck, A., 2010. New particle formation events measured on board the ATR-42 aircraft during the EUCAARI campaign. Atmos. Chem. Phys. 10, 6721–6735. http://dx.doi.org/10.5194/acp-10-6721-2010.
Cubison, M.J., Ervens, B., Feingold, G., Docherty, K.S., Ulbrich, I.M., Shields, L., Prather, K., Hering, S., Jimenez, J.L., 2008. The influence of chemical composition and mixing state of Los Angeles urban aerosol on CCN number and cloud properties. Atmos. Chem. Phys. 8, 5649–5667.
Drewnick, F., Schneider, J., Hings, S.S., Hock, N., Noone, K., Targino, A., Weimer, S., Borrmann, S., 2007. Measurement of ambient, interstitial, and residual aerosol particles on a mountain-top site in Central Sweden using an Aerosol Mass Spectrometer and a CVI. J. Atm. Chem. 56, 1–20. http://dx.doi.org/10.1007/s10874-006-9036-8.
Drewnick, F., Hings, S.S., DeCarlo, P.F., Jayne, J.T., Gonin, M., Fuhrer, K., Weimer, S., Jimenez, J.L., Demerjian, K.L., Borrmann, S., Worsnop, D.R., 2005. A new time-of-flight aerosol mass spectrometer (ToF-AMS) – instrument description and first field deployment. Aerosol Sci. Technol. 39, 637–658.
Feingold, G., Stevens, B., Cotton, W.R., 1998. Simulations of marine stratocumulus using a new microphysical parameterization. Atmos. Res. 47-48, 505–528.
Feingold, G., Kreidenweis, S.M., Stevens, B., Cotton, W.R., 1996. Numerical simulations of stratocumulus processing of cloud condensation nuclei through collision-coalescence. J. Geophys. Res. 101, 21,391–21,402.
Fitzgerald, J., Martin, J.J., Hoppel, W.A., Frick, G.M., Gelbard, J., 1998. A one-dimensional sectional model to simulate multi-component aerosol dynamics in the marine boundary layer, 2, Modeling application. J. Geophys. Res. 103, 16,103–16,117.
Flossmann, A.I., Hall, W.D., Pruppacher, H.R., 1985. A theoretical study of the wet removal of atmospheric pollutants: Part I. The redistribution of aerosol particles captured through nucleation and impaction scavenging by growing cloud drops. J. Atmos. Sci. 42, 582–606.
Harrison, R.G., 2000. Cloud formation and the possible significance of charge for atmospheric condensation and ice nuclei. Space Sci. Rev. 94, 381–396.
Hartmann, D., Ockert-Bell, M., Michelsen, M., 1992. The effect of cloud type on earth's energy balance: global analysis. J. Clim. 5, 1281–1304.
Hayden, K.L., Macdonald, A.M., Gong, W., Toom-Sauntry, D., Anlauf, K.G., Leithead, A., Li, S.-M., Leaitch, W.R., Noone, K., 2008. Cloud processing of nitrate. J. Geophys. Res. 113, D18201. http://dx.doi.org/10.1029/2007JD009732.
Haywood, J., Francis, P., Osborne, S., Glew, M., Loeb, N., Highwood, E., Tanre′, D., Myhre, G., Formenti, P., Hirst, E., 2003. Radiative properties and direct radiative effect of Saharan dust measured by the C-130 aircraft during SHADE: 1. Solar spectrum. J. Geophys. Res. 108 (D18), 8577. http://dx.doi.org/10.1029/2002JD002687.
Hegg, D.A., Radke, L.F., Hobbs, P.V., 1990. Particle production associated with marine clouds. J. Geophys. Res. 95, 13,917–13,926.
Hegg, D.A., 1985. The importance of liquid-phase oxidation of $SO_2$ in the troposphere. J. Geophys. Res. 90 (D2), 3773–3779.
Hegg, D.A., Hobbs, P.V., 1982. Measurement of sulfate production in natural clouds. Atmos. Environ. 16, 2663–D2668.
Hinds, W.C., 1998. Aerosol Technology: Properties, Behavior, and Measurement of Airborne Particles, second ed. John Wiley, New York.
Hoppel, W.A., Frick, G.M., Fitzgerald, J.W., Larson, R.E., 1994. Marine boundary layer measurements of new particle formation and the effects nonprecipitating clouds have on aerosol size distribution. J. Geophys. Res. 99 (D7), 14,443–14,459. http://dx.doi.org/10.1029/94JD00797.
Hoppel, W.A., Frick, G.M., Larson, R.E., 1986. Effects on non-precipitating clouds on the aerosol size distribution in the marine boundary layer. Geophys. Res. Lett. 13, 125–128.
Huffman, J.A., Jayne, J.T., Drewnick, F., Aiken, A.C., Onasch, T., Worsnop, D.R., Jimenez, J.L., 2005. Design, modeling, optimization, and experimental tests of a particle beam width probe for the aerodyne aerosol mass spectrometer. Aerosol Sci. Technol. 39, 1143–1163.
IPCC: Intergovernmental Panel on Climate Change, 2007. ClimateChange 2007 – the Physical Science Basis: Contribution ofWorking Group I to the Fourth Assessment Report of the IPCC. Cambridge University Press, Cambridge.
Jaffrezo, J.-L., Aymoz, G., Cozic, J., 2005. Size distribution of EC and OC in the aerosol of Alpine valleys during summer and winter. Atmos. Chem. Phys. 5, 2915–2925. http://dx.doi.org/10.5194/acp-5-2915-2005.
Jiang, H., Feingold, G., Cotton, W.R., 2002. Simulations of aerosol–cloud-dynamical feedbacks resulting from entrainment of aerosol into the marine boundary layer during the Atlantic Stratocumulus transition Experiment. J. Geophys. Res. 107 (D24), 4813. http://dx.doi.org/10.1029/2001JD001502.
Jimenez, J.L., Jayne, J.T., Shi, Q., Kolb, C.E., Worsnop, D.R., Yourshaw, I., Seinfeld, J.H., Flagan, R.C., Zhang, X., Smith, K.A., Morris, J., Davidovits, P., 2003. Ambient aerosol sampling with an aerosol mass spectrometer. J. Geophys. Res. Atmospheres 108 (D7), 8425. http://dx.doi.org/10.1029/2001JD001213.
Joos, F., Baltensperger, U., 1991. A field study on chemistry, S(IV) oxidation rates and vertical transport during fog conditions. Atmos. Environ. Part A. Gen. Top. 25 (2), 217–230. http://dx.doi.org/10.1016/0960-1686(91)90292-F.
Karamchandani, P., Venkatram, A., 1992. The role of non-precipitating clouds in producing ambient sulfate during summer: results from simulations with the acid deposition and oxidant model (ADOM). Atmos. Environ. 26A (6), 1041–1052.
Katrib, Y., Martin, S., Rudich, Y., Davidovits, P., Jayne, J., Worsnop, D., 2005. Density changes of aerosol particles as a result of chemical reactions. Atmos. Chem. Phys. 5, 275–291.
Kaufman, Y.J., Tanre, D., Boucher, O., 2002. A satellite view of aerosols in the climate system. Nature 419, 215–223.
Komppula, M., Lihavainen, H., Kerminen, V., Kulmala, M., Viisanen, Y., 2005. Measurements of cloud droplet activation of aerosol particles at a clean subarctic background site. J. Geophys. Res. 110, D06204. http://dx.doi.org/10.1029/2004JD005200.
Kulmala, M., Asmi, A., Lappalainen, H.K., Carslaw, K.S., Pöschl, U., Baltensperger, U., Hov, Ø., Brenquier, J.-L., Pandis, S.N., Facchini, M.C., Hansson, H.-C., Wiedensohler, A., O'Dowd, C.D., 2009. Introduction: European Integrated Project on Aerosol Cloud Climate and Air Quality interactions (EUCAARI) – integrating aerosol research from nano to global scales. Atmos. Chem. Phys. 9, 2825–2841.
Kulmala, M., Asmi, A., Lappalainen, H.K., Baltensperger, U., Brenguier, J.-L., Facchini, M.C., Hansson, H.-C., Hov, Ø., O'Dowd, C.D., Pöschl, U., Wiedensohler, A., Boers, R., Boucher, O., de Leeuw, G., Denier van den Gon, H., Feichter, J., Krejci, R., Laj, P., Lihavainen, H., Lohmann, U., McFiggans, G., Mentel, T., Pilinis, C., Riipinen, I., Schulz, M., Stohl, A., Swietlicki, E., Vignati, E., Amann, M., Amann, M., Alves, C., Arabas, S., Artaxo, P., Beddows, D.C.S., Bergström, R., Beukes, J.P., Bilde, M., Burkhart, J.F., Canonaco, F., Clegg, S., Coe, H., Crumeyrolle, S., D'Anna, B., Decesari, S., Gilardoni, S., Fischer, M., Fjæraa, A.M., Fountoukis, C., George, C., Gomes, L., Halloran, P., Hamburger, T., Harrison, R.M., Herrmann, H., Hoffmann, T., Hoose, C., Hu, M., Hõrrak, U., Iinuma, Y., Iversen, T., Josipovic, M., Kanakidou, M., Kiendler-Scharr, A., Kirkevåg, A., Kiss, G., Klimont, Z., Kolmonen, P., Komppula, M., Kristjánsson, J.-E., Laakso, L., Laaksonen, A., Labonnote, L., Lanz, V.A., Lehtinen, K.E.J., Makkonen, R., McMeeking, G., Merikanto, J., Minikin, A., Mirme, S., Morgan, W.T., Nemitz, E., O'Donnell, D., Panwar, T.S., Pawlowska, H., Petzold, A., Pienaar, J.J., Pio, C., Plass-Duelmer, C., Prévôt, A.S.H., Pryor, S., Reddington, C.L., Roberts, G., Rosenfeld, D., Schwarz, J., Seland, Ø., Sellegri, K., Shen, X.J., Shiraiwa, M., Siebert, H., Sierau, B., Simpson, D., Sun, J.Y., Topping, D., Tunved, P., Vaattovaara, P., Vakkari, V., Veefkind, J.P., Visschedijk, A., Vuollekoski, H., Vuolo, R., Wehner, B., Wildt, J., Woodward, S., Worsnop, D.R., van Zadelhoff, G.-J., Zardini, A.A., Zhang, K., van Zyl, P.G., Kerminen, V.-M., S. Carslaw, K., Pandis, S.N., 2011. General overview: European Integrated project on Aerosol Cloud Climate and Air Quality interactions (EUCAARI) – integrating aerosol research from nano to global scales. Atmos. Chem. Phys. Discuss. 11, 17941–18160. http://dx.doi.org/10.5194/acpd-11-17941-2011.
Leaitch, W.R., Strapp, J.W., Wiebe, H.A., Anlauf, K.G., Isaac, G.A., 1986. Chemical and microphysical studies of nonprecipitating summer cloud in Ontario, Canada. J. Geophys. Res. 91, 11821–11831.
Leriche, M., Curier, R.L., Deguillaume, L., Caro, D., Sellegri, K., Chaumerliac, N., 2007. Numerical quantification of sources and phase partitioning of chemical species in cloud: application to wintertime anthropogenic air masses at the Puy de Dôme station. J. Atmos. Chem. 57 (3), 281–297. http://dx.doi.org/10.1007/s10874-007-9073-y.
Levin, Z., Ganor, E., Gladstein, V., 1996. The effects of desert particles coated with sulfate on rain formation in the eastern mediterranean. J. Appl. Meteorol. 35, 1511–1523.
Liu, P.S.K., Deng, R., Smith, K.A., Williams, L.R., Jayne, J.T., Canagaratna, M.R., Moored, K., Onasch, T.B., Worsnop, D.R., Deshler, T., 2007. Transmission efficiency of an aerodynamic focusing lens system: comparison of model calculations and laboratory measurements for the Aerodyne aerosol mass spectrometer. Aerosol Sci. Technol. 41, 721–733.
Lohmann, U., Broekhuizen, K., Leaitch, R., Shantz, N., Abbatt, J., 2004. How efficient is cloud droplet formation of organic aerosols? Geophys. Res. Lett. 31, L05108 http://dx.doi.org/10.1029/2003GL018 999.
Matsuki, A., Schwarzenboeck, A., Venzac, H., Laj, P., Crumeyrolle, S., Gomes, L., 2010. Cloud processing of mineral dust: direct comparison of cloud residual and clear sky particles during AMMA aircraft campaign in summer 2006. Atmos. Chem. Phys. 10, 1057–1069.
Matthew, B.M., Middlebrook, A.M., Onasch, T.B., 2008. Collection efficiencies in an Aerodyne aerosol mass spectrometer as a function of particle phase for laboratory generated aerosols. Aerosol Sci. Technol. 42 (11), 884–898. http://dx.doi.org/10.1080/02786820802356797.
McNaughton, C.S., Clarke, A.D., Howell, S.G., Pinkerton, M., Anderson, B., THornhill, L., Hudgins, C., Winstead, E., Dibb, J.E., Sceuer, E., Maring, H., 2007. Results from the DC-8 inlet characterization experiment (DICE): airborne versus surface sampling of mineral dust and sea salt aerosols. Aerosol Sci. Technol. 41, 136–159.
Middlebrook, A.M., Bahreini, R., Jimenez, J.L., Canagaratna, M.R., 2012. Evaluation of composition-dependent collection efficiencies for the Aerodyne aerosol mass spectrometer using field data. Aerosol Sci. Technol. 46, 258–271. http://dx.doi.org/10.1080/02786826.2011.620041.
Mirme, S., Mirme, A., Minikin, A., Petzold, A., Hõrrak, U., Kerminen, V.-M., Kulmala, M., 2010. Atmospheric sub-3 nm particles at high altitudes. Atmos. Chem. Phys. 10, 437–451.
Murphy, D.M., Thomson, D.S., Mahoney, M.J., 1998. In situ measurements of organics, meteoritic material, mercury, and other elements in aerosols at 5 to 19 kilometers. Science 282, 1664–1669.
Ogren, J.A., Heintzenberg, J., Charlson, R.J., 1985. In-situ sampling of clouds with a droplet to aerosol converter. Geophys. Res. Lett. 12, 121–124.

Philippin, S., Laj, P., Putaud, J.-P., Wiedensohler, A., de Leeuw, G., Fjaeraa, A.M., Platt, U., Baltensperger, U., Fiebig, M., 2009. EUSAAR – an unprecedented network of aerosol observation in Europe. Earozoru Kenkyu, JAAST 24 (2), 78–83.

Plaza, J., Pujadas, M., Gómez-Moreno, F.J., Sánchez, M., Artíñano, B., 2011. Mass size distributions of soluble sulfate, nitrate and ammonium in the Madrid urban aerosol. Atmos. Environ.. ISSN: 1352-2310 45 (28), 4966–4976. http://dx.doi.org/10.1016/j.atmosenv.2011.05.075.

Protat, A., Pelon, J., Testud, J., Grand, N., Delville, P., Laborie, P., Vinson, J.-P., Bouniol, D., Bruneau, D., Chepfer, H., Delanoë, J., Haeffelin, M., Noël, V., Tinel, C., 2004. Le projet RALI: Combinaison d'un radar nuage et d'un lidar pour l'étude des nuages faiblement précipitants. La Météorologie 47 (2004), 23–33.

Pruppacher, H.R., Klett, J.D., 1997. Microphysics of Clouds and Precipitation. Kluwer Academic Publishers, Dordrecht, p. 954.

Reutter, P., Su, H., Trentmann, J., Simmel, M., Rose, D., Gunthe, S.S., Wernli, H., Andreae, M.O., Pöschl, U., 2009. Aerosoland updraft-limited regimes of cloud droplet formation: influence of particle number, size and hygroscopicity on the activation of cloud condensation nuclei (CCN). Atmos. Chem. Phys. 9, 7067–7080. http://dx.doi.org/10.5194/acp-9-7067-2009.

Roberts, G.C., Andreae, M.O., Zhou, J., Artaxo, P., 2001. Cloud condensation nuclei in the Amazon Basin: marine conditions over a continent? Geophys. Res. Lett. 28 (14), 2807–2810.

Saxena, V.K., 1996. Bursts of cloud condensation nuclei (CCN) by dissipating clouds at Palmer Station, Antarctica. Geophys. Res. Lett. 23, 69–72.

Schwarzenboeck, A., Heintzenberg, J., Mertes, M., 2000. Incorporation of aerosol particles between 25 and 850 nm into cloud elements: measurements with a new complementary sampling system. Atmos. Res. 52, 241–260.

Seigneur, C., Saxena, P., 1988. A theoretical investigation of sulfate formation in clouds. Atmos. Environ. 22, 101–115.

Seinfeld, J.H., Pandis, S.N., 1998. Atmospheric Chemistry and Physics. Wiley-Interscience, New York, p. 1326.

Sellegri, K., Laj, P., Dupuy, R., Legrand, M., Preunkert, S., Putaud, J.-P., Cachier, H., 2003. Size-dependent scavenging efficiencies of multi-component atmospheric aerosols in clouds. J. Geophys. Res. 108 (D11), 4334–4349. http://dx.doi.org/10.1029/2002JD002749.

Slowik, J.G., Stainken, K., Davidovits, P., Williams, L.R., Jayne, J., Kolb, C.E., Worsnop, D., Rudich, Y., DeCarlo, P., Jimenez, J., 2004. Particle morphology and density characterization by combined mobility and aerodynamic diameter measurements. Part 2: application to combustion generated soot particles as a function of fuel equivalence ratio. Aerosol Sci. Technol. 28 (12), 1206–1222.

Spichtinger, P., Cziczo, D.J., 2008. Aerosol–cloud interactions—a challenge for measurements and modeling at the cutting edge of cloud–climate interactions. Environ. Res. Lett. 3, 025002. http://dx.doi.org/10.1088/1748–9326/3/2/025002.

Stohl, A., Forster, C., Frank, A., Seibert, P., Wotawa, G., 2005. Technical note: the Lagrangian particle dispersion model FLEXPART version 6.2. Atmos. Chem. Phys. 5, 2461–2474.

Stohl, A., Hittenberger, M., Wotawa, G., 1998. Validation of the Lagrangian particle dispersion model FLEXPART against large scale tracer experiment data. Atmos. Environ. 24, 42454264.

Stroud, C.A., Nenes, A., Jimenez, J.L., DeCarlo, P.F., Huffman, J.A., Bruintjes, R., Nemitz, E., Delia, A.E., Toohey, D.W., Guenther, A.B., Nandi, S., 2007. Cloud activating properties of aerosol observed during CELTIC. J. Atmos. Sci. 64, 441–459. http://dx.doi.org/10.1175/JAS3843.1.

Sturman, A.P., McGowan, H.A., 1995. An assessment of boundary-layer air mass characteristics associated with topographically-induced local wind systems. Bound. Layer Meteor. 74, 181–193.

Sun, J., Zhang, Q., Canagaratna, M.R., Zhang, Y., Ng, N.L., Sun, Y., Jayne, J.T., Zhang, X., Worsnop, D.R., 2010. Highly time- and size-resolved characterization of submicron aerosol particles in Beijing using an Aerodyne Aerosol Mass Spectrometer. Atmos. Environ. 44 (1), 131–140. http://dx.doi.org/10.1016/j.atmosenv.2009.03.020.

Twohy, C.H., Strapp, J.W., Wendisch, M., 2003. Performance of a counterflow virtual impactor in the NASA icing research tunnel. J. Atmos. Oceanic Tech. 20, 781–790.

Venzac, H., Sellegri, K., Laj, P., 2007. Nucleation events detected at the high altitude site of the Puy de Dôme research Station, France. Boreal Env. Res. 12, 345–359.

Villani, P., Picard, D., Marchand, N., Laj, P., 2007. Design and Validation of a Volatility Tandem Differential Mobility Analyzer (VTDMA). Aerosol Sci. Technol. 41 (10), 898–906.

Vocourt, V., 2002. Etalonnage et Simulation numerique d'une Sonde a Impaction Virtuelle (CVI) dans le cadre de l'etude des proprietes physico-chimiques des particules nuageuses. Ph.D. thesis. Blaise Pascal, Clermont Ferrand.

Walcek, C.J., Taylor, G.R., 1986. A theoretical method for computing vertical distributions of acidity and sulfate production within cumulus clouds. J. Atmos. Sci. 43 (4), 339–355.

Wall, S.M., John, W., Ondo, J.L., 1988. Measurement of aerosol size distributions for nitrate and major ionic species. Atmos. Environ.. ISSN: 0004-6981 22 (8), 1649–1656. http://dx.doi.org/10.1016/0004-6981(88)90392-7.

Wang, M., Ghan, S., Easter, R., Ovchinnikov, M., Liu, X., Kassianov, E., Qian, Y., Gustafson Jr., W.I., Larson, V.E., Schanen, D.P., Khairoutdinov, M., Morrison, H., 2011. The multi-scale aerosol-climate model PNNL-MMF: model description and evaluation. Geosci. Model Dev. 4, 137–168. http://dx.doi.org/10.5194/gmd-4-137-2011.

Warren, S., Hahn, C., London, J., Chervin, R., Jenne, R., 1988. Global Distribution of Total Cloud Cover and Cloud Type Amounts over the Ocean. Tech. Note NCAR/TN- 317_STR. NCAR, p. 42.

Weber, R.J., McMurry, P.H., 1996. Fine particle size distributions at the Mauna Loa observatory, Hawaii. J. Geophys. Res. 101 (D9), 14,767–14,775. http://dx.doi.org/10.1029/95JD02271.

Wurzler, S., Reisin, T.G., Levin, Z., 2000. Modification of mineral dust particles by cloud processing and subsequent effects on drop size distributions. J. Geophys. Res. 105 (D5), 4501–4512.

Zhang, Q., Canagaratna, M.C., Jayne, J.T., Worsnop, D.R., Jimenez, J.L., 2005. Time and size- resolved chemical composition of submicron particles in Pittsburgh—implications for aerosol sources and processes. J. Geophys. Res. 110. http://dx.doi.org/10.1029/2004JD004649.

Zhang, X., Smith, K.A., Worsnop, D.R., Jimenez, J.L., Jayne, J.T., Kolb, C.E., Morris, J., Davidovits, P., 2004. Numerical characterization of particle beam collimation: part II integrated aerodynamic lens-nozzle system. Aerosol Sci. Tech. 38 (6), 619–638.